International Journal on Interactive Design and Manufacturing (IJIDeM)
https://doi.org/10.1007/s12008-026-02521-9

ORIGINAL ARTICLE

Machinability of LM 25 cast composites using hybrid nano coolant: optimization of cutting parameters by RSM and evolutionary algorithm

Virupakshappa S. Konnur[1] · Aravindkumar D. Kotagond[1] · Basavaraj M. Angadi[1] · Vishwanath S. Kanal[1] · Kailash S. Chadchan[2]

Received: 15 September 2025 / Revised: 20 January 2026 / Accepted: 7 February 2026

Abstract

The research topic is selected to address the performance of LM 25 AHMMC cast composites. The selected material is widely utilised in automobiles, aerospace, and marine parts as an alternative to piston material. The cast composites are prepared by reinforcement of $nTiO_2$, $nZrO_2$, and bagasse ash materials in different combinations of wt% to LM 25. The 84% LM 25, and 5% $nTiO_2$ + 3% $nZrO_2$ + 8% bagasse ash combination exhibits 96.20 HV microhardness with an improvement in hardness by 38.76 HV compared to the base alloy. The objective of the research is to study the surface roughness, rate of material removed, insert tip temperature, flank wear, and feed force in the turning process. The RSM is used to develop the test combinations using speed, feed, hardness of cast composite, and cooling environment as variables in three levels by keeping depth constant. The soybean oil is utilised to prepare nano coolant by concentrating the $nTiO_2$, $nMoS_2$, and nZnO materials with different wt% combinations used in MAC condition. The TiCN- and Al_2O_3-coated inserts are used to investigate the performance in terms of flank wear. The variables are analyzed by statistical tools DFA and RSM and soft tools MOGA, MOPSO, and MONSG2. The lowest SR of 2.4 μm, 32.59 °C of ITT, and 1.2 kgf feed force are generated by MOGA for M1, M3, and M1 cast composites, respectively, for the NC-2 cooling environment, and 0.0032 mm flank wear by MOPSO for M2 and cast composites in the NC-1 cooling environment are studied through the Pareto front.

✉ Virupakshappa S. Konnur
mech.virupax@bldeacet.ac.in

[1] Faculty Department of Mechanical Engineering, BLDEA's V. P. Dr. P. G. Halakatti College of Engineering and Technology, (Affiliated to Visvesvaraya Technological University, Belagavi-590018), Vijayapura, Karanataka 586103, India

[2] Faculty Department of Chemistry, BLDEA's V. P. Dr. P. G. Halakatti College of Engineering and Technology, (Affiliated to Visvesvaraya Technological University, Belagavi-590018), Vijayapura, Karanataka 586103, India

Published online: 11 March 2026

Graphical abstract

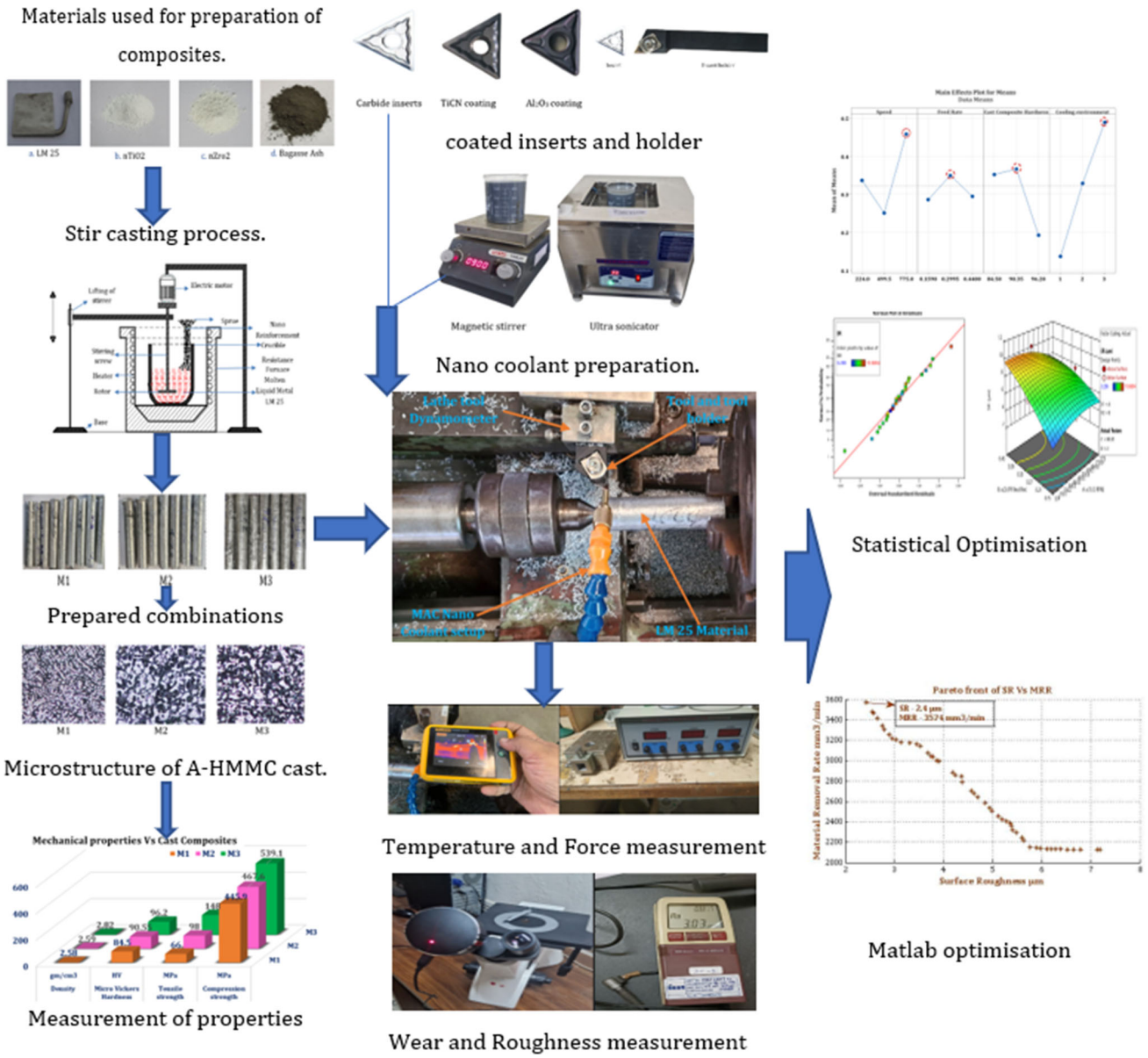

Keywords LM 25 alloy · Nano Coolant · SR · MRR · Insert Tip Temperature · Insert Flank wear · DFA · MOGA · MOPSO · NSG2 · RSM

Abbreviations

SR	Surface Roughness
LM	Liquid Metal
MRR	Material Removal Rate
S	Speed
DOC	Depth of Cut
FR	Feed Rate
MOGA	Multi Objective Genetic Algorithm
RSM	Response Surface Methodology
BBD	Box-Behnken Design
C	Coating
ITT	Insert Tip Temperature
NC	Nano coolant
MAC	Minimum Amount of Coolant
OF	Objective function
w/p	Work piece
A	Aluminum

HMMC	Hybrid Metal Matrix Composite
MOPSO	Multi Objective Particle Swarm Optimisation
NSG	Non-Dominated sorting Genetic algorithm
IFW	Insert Flank Wear
FF	Feed Force
DFA	Desirability Function Analysis

1 Introduction

The aluminum is a low-weight material and nonferrous. The aluminum composites are prepared by mixing the different materials with aluminum base. Now a days the hybrid metal matrix composites are developing to check the current requirements of engineering applications. Due to the benefits of A-HMMC in the field of engine parts, marine, aerospace, and automobile parts, the study of A-HMMC plays a very important role. The filler materials play a very effective role in composites, which improves the hardness, compression strength, toughness, wear resistance, etc., compared to the base aluminum. The stir casting method is the best method for the preparation of composite materials, which also improves the thermal properties along with other properties.

The hybrid aluminum composites were studied to exhibit a significant role in wear resistance and tribological properties of the materials. A356 material is squeeze stir cast with MoS_2 and silicon carbide by varying pressure to improve the properties of composites. At 120 MPa a fine microstructure, and better wear and friction resistance were observed [1]. LM 26 material is reinforced with fly ash and graphite by the stir cast process to improve the strength and hardness of the prepared composite material. Material with 7.5% fly ash and graphite provides the best hardness and tensile strength. The wear and microstructural study were done by regression analysis [2]. The wear and friction behaviour of LM 25 HMMC was studied by reinforcing the HBn and boron carbide with different percentages. The study is carried out on pin on disc under dry conditions. The 6% boron carbide and 2% HBn exhibit low friction and wear [3].

The fly ash, titanium dioxide, and B_4C were reinforced with aluminum 7178 through stir casting to study the wear behavior. The RSM-CCD is used in experimental process to study the wear of the composite material. The load, speed, and distance of sliding were used as input parameters. ANOVA shows that the sliding distance and the load are the most significant parameters that affects the wear [4]. The LM 25 is reinforced with 2.5 wt.% of TiO_2 and 7.5 wt.% of silicon carbide by the stir cast process. The energy spectroscopy and microstructural processes were used to study the quality of reinforcement. The ED machining process is incorporated for the study of surface roughness and MRR, using pulse on-time, voltage, and current as input factors. The ANOVA and GRA techniques were used for optimisation of results [5]. An abrasive wear test was conducted on HMMC specimens, prepared by mixing 10% TiC with LM 25. The speed, load, and time were considered as input parameters by using RSM. Regression models developed for confirming accuracy. The minimum wear was observed at 27N load [6].

Using the stir casting method, LM25 is mixed with ZrO2, Al2O3, SiO2, MgO Gr in different weight percentages. The mechanical properties were studied. The composition and morphology were studied using SEM, EDX, and XRD [7]. The mechanical properties and reinforcement of LM25 were studied by the MDF process. The material is solutionized in water for 10 h at 535 °C and quenched in the water. Improvement in hardness and tensile strength was improved [8]. The SiC and TiO2 reinforced with LM25 material. The prepared composite material is heat treated, quenched in water and artificially aged with different times. The heat treatment effect was studied by hardness and microstructure study. The pulse on time, aging times, cutting speed, and wire feed rate were taken as input parameters in the WEDM process to study [9].

The combinations of hybrid nanoparticles were used in base fluid. ZnO, AIN, and hBN nanomaterials were selected due to their thermal characteristics. hBN, hBn and AIN, hBN, and AIN and ZnO mixtures with 3 different combinations were mixed with coconut oil as a base fluid. The nanofluid as MQL is used in the turning process on SS304 material. The optimal tool wear and surface roughness were obtained by hybrid nano fluid mixture in comparison with dry and single mixtures of nanofluid [10]. The Al_2O_3 nanomaterial with a 60 nm size is selected and mixed with coconut oil as a base fluid. The nanomaterial is mixed with base oil in 6 different weight proportions ranging from 0.5% to 1.5%. The turning tests were conducted on AISI 1040 steel with flood, MQL dry, and nanofluid as a cooling environment. The outcomes are better by using nanofluid and wear, roughness were decreased by using nanofluid [11].

The vegetable oil exhibits poor oxidation and thermal stability at elevated temperatures; hence, vegetable oil is used as a coolant. The Al_2O_3 nanoparticles with 0.25% to 1.5% weight percentage were added with coconut oil, and nanofluid was prepared. The dry, flood cooling, only coconut oil, and NF MQL environment were used in the turning of AISI 1040 steel. NF MQL provides superior results compared to the other cooling environment, by increasing the tool life, and reducing the wear, temperature, and roughness [12]. The Al_2O_3 with particle size 20–30 nm and TiO_2 with 20–25 nm particle size were mixed with SAE engine oil with different weight proportion, and the nanofluid and used as MQL method. These nanofluid mixtures were used in the turning of Inconel 718 material. The roughness reduced at 0.5 gm nanomaterial with 100 gm oil mixture nanofluid [13]. The soybean and emulsion oils were used as base oils

for preparing nano coolant. The Al_2O_3 and MoS_2 nanoparticles with an average size of 30 nm particle size were mixed with oils and prepared nano coolants. The turning tests were conducted on 90CrSi steel by using nano coolant. The Al_2O_3 nanofluid provides less surface roughness compared to MoS_2 nano fluid [14].

The pure vegetable-based oil, without any chemical composition was used as base oil and Al_2O_3 nanoparticles with 22 nm were mixed in 0, 2, and 4 weight percentages. This both prepared nanofluid were used in turning of Ti-6Al-4 V material by considering different input parameters. The adhesion of the material and tool interface was reduced by using MQL nanofluid by comparing it to MQL normal oil as a coolant. The nano fluid with 2 percentage weight provides better performance [15]. The radiator coolant was selected as the base coolant and the graphene nanomaterial was concentrated to prepare nanofluid. This prepared nano coolant is used in the turning of AISI D3 steel. The NFMQL used was exhibits the best cooling effects by improving the machining cost and reducing temperature [16].

The emulsified fluid is used as a base fluid, the CuO and Al_2O_3 nanoparticles, having a 30–50 nm particle size with different weight percentages were mixed with the base fluid to form a nano coolant. The prepared coolant is used in the turning of Duplex Stainless Steel. The Al_2O_3 nanofluids improve the finishing and reduce the forces in comparison with CuO nanofluid [17]. The Eraoil KT vegetable oil was selected as the base oil, hBN and MWCNT nan powders were used for the preparation of nanofluid. Two separate hBN nano fluid and MWCNT nanofluids were prepared. The fluids were used in the turning of AISI H11 steel in MQL condition. In a comparison of both fluids, the nano MWCNT exhibits the lowest roughness and temperature [18].

A biodegradable oil CUTTEX SYN-10 was used as a base oil for the preparation of nanofluid. The 1% weight of MWCNT, 8–10 nm particle size, was used. The prepared nanofluid is used in MQL environment. The experiment was conducted on AZ91D alloy in dry, base oil, nanofluid conditions with varying input parameters. The nano cooling condition provides superior thermal conductivity and reduced force during the turning process [19]. A 250 ml glycerol and 750 ml deionized water concentration was used for nano coolant preparation. The first mixture was 1.92 gm of Al_2O_3, 0.13 gm of graphene with 0.5% concentration and the second one was 0.25 gm graphene, and 3.75 gm Al_2O_3 with 1% concentration, and the third was 0.375 gm graphene and 5.625 gm Al_2O_3 with 1.5% concentration was selected. The prepared nano coolant was used in turning of AISI D2 steel. 1.5% concentration exhibits the best performance [20].

A sunflower oil was selected for preparation of nano coolant by mixing alumina nano powder of 40 nm particle size. The concentration varied from 0 to 1 percent. The prepared nano coolant was used to cut Inconel 690 material in turning. The 0.8% concentration provides reduced roughness temperature and cutting force [21]. A KT-2000 synthetic oil is concentrated with 0.5% cellulose nanocrystal and nano graphene in weight percentage. This nanofluid is used in the turning of UHSS S1100 material under dry, the MQL, nano MQL conditions. This provides a decrease in tool wear and temperature [22].

Al_2O_3 with 30–50 nm particle size was selected for preparation of nanofluid. 95% emulsion & 5% servo cuts oil was selected. A 0.1% weight concentration is selected for nanofluid preparation. The Grade 40 mild steel was used for the turning experiment. This coolant improves the machining stability and efficiency of cooling by reducing wear of the tool and roughness [23]. The heat transfers by using nanofluid depends on particle size, shape, quantity, surfactant, etc. The conductivity of different nanoparticles was collected. The preparation of nano coolant and methods was explained in the review. The purpose of surfactants was reviewed [24].

The MWCNT is doped with soybean oil to prepare nanofluid. The 4 different environmental conditions were used for the machining operation. The surface roughness, and flank wear were studied for all four conditions. The N MQL provides better results compared to other conditions. [25]. Wet, MQL soybean oil, and Dry cooling conditions were used in the turning of Ti-6Al-4 V alloy. As compared to dry and wet conditions MQL soybean oil exhibits reduced roughness and wear during the turning process [26]. The vegetable cutting fluid and its effect on machining operations were reviewed. The review indicates that the vegetable oils can replace the regular coolant. Also reviewed the different biodegradable oil with additives and methodology [27]. The different mineral-based and vegetable based cutting fluids were reviewed. The method of preparation and additives used in nanofluid were reviewed [28].

The different PVD-coated tools were used in the turning of AISI 316L steel. The TiN and TiAlN coted tools were used. The coated tool temperatures were studied during machining. The highest temperature was observed in the uncoated tool compared to the coated tool [29]. CVD-coated cemented carbide tools were used in the turning of AISI 316Ti material. The 1 μm thickness of Al2O3/Ti (C, N) coated tools was used to study the notch wear. In comparison of κ-Al2O3-TiN and α-Al2O3/Ti (C, N) coated tools α-Al2O3/Ti (C, N) coated tool provides small notch wear [30]. The TiAlN-PVD coated tools were used in the turning of C276 Hastelloy. The Al nanofluid with MQL condition was used in machining. The nano fluid reduces the tool wear. [31]. The TiCN/Al2O3/TiN multi-layered tungsten carbide tools were used in the turning of AL MMC. Increased power consumption and vibration was observed at higher speed; the reduced roughness was observed at higher nose radius. [32]. The PVD TiAlN coated carbide inserts with thickness of 1 μm and 2 μm were used in the turning of Inconel 718. The thinner coating provides

reduced temperature as compared to the thicker coating at the same speed. And also exhibits lower wear of the tool [33].

The SiCp/Al MMC was used in turning with coated inserts for wear measurement. Al2O3/TiCN was coated on the rake face whereas TiN/Al2O3/TiNC on the flank face was made. The CVD coated tool reduces the wear [34]. TiNAl or AlCrN over TiNAl—AlCrN + coated cemented carbide tools with different cutting environments were used in turning of Inconel 718. AlCrN + with cooling conditions exhibits higher MRR and lower wear [35]. Three different PVD coated inserts were used in the turning of Ti-5Al-5 V-5Mo-3Cr alloy. The commercial AlTiN, AlCrN were used for both dry and wet conditions, and TiAl-SiN was used. The study was focused on tool life and roughness of all coatings. AlTiN/AlCrN coated tool exhibited the longest tool life and fine surface finish [36]. TiN-coated tungsten carbide tools along with nAl_2O_3 and palm oil mixture nanofluids in MQL condition were used in the turning of Inconel 718. The 0.8 wt% addition of Al_2O_3 and palm oil mixture exhibits better tool life, and reduced wear and roughness [37].

The TiCN, TiAlN, and Al_2O_3 coated tools were used for dry turning with different speeds. The tool coating effectively reduces the temperature and force of cutting. The Al_2O_3 coated tools provide better reduction in temperature. TiCN provides better wear resistance [38]. The TiAlSiN PVD coated tungsten carbide tools were used in the turning of custom 450 steel. The cutting force was studied on coated tools. The GWO, PSO, and WOA algorithms were used for optimization of force [39]. The CVD TiCN-Al2O3 coated inserts were used in dry turning of SDSS 2507 material. The cutting force, wear and roughness were studied by coated tool. [40]. The AlTiSiN and AlTiN coated two different tools were used in the turning of AISI H10 steel. AlTiSiN coated tools were better at reducing temperature, force, wear, and roughness. The tool life for this coating is much better in comparison with others [41]. The TiAlN/CrN bilayer coated tools were used in the turning of 316 LVM steel. RSM and ANOVA were used for optimizing the results. The tool wear was studied by coated tool by using FEM [42].

Cu-Al-Mn alloy steel is in the turning operation by using different coated carbide tools. A multilayer coating of Al_2O_3, TiN, and TiCN material was used on tools. Higher speed results in an increase of the MRR and cutting force. As feed rate an increase the forces increase. The SR is higher at the lowest speed [43]. The cutting models and tool wear were predicted by a high-feed turning machine by turning C263 superalloy. Mainly CO_2, oil emulsion cooling effect and reduction of side cutting angles were studied. The tool life was increased, and tool wear was reduced by side cutting angle reduction [44]. The coated carbide tools were used in the turning of AISI 4140 steel. A multilayered Al_2O_3- TiCN coating was done on carbide tools. The feed rate was most influenced by cutting force and roughness values [45]. The effect of tool wear was studied in the turning of hardened AISI5200 steel in finish turning. The RSM, MSE, etc., were used for planning and optimisation. The flack wear was significant with roughness. At higher cutting times the lower roughness was observed with maximum robustness [46]. The Inconel 800 super alloy is used in dry turning to study the flank wear and roughness by using uncoated inserts. The Taguchi's technique is used for experiments, and GRA, and ANOVA were used for optimisation of parameters. Diffusion, adhesion, and abrasion wear were observed [47].

The MQL hard turning of 90CrSi steel was done by CBN tools in dry, nAl2O3, nAl2O3 & nMoS2 hybrid environment conditions. The soybean oil is considered as a base oil for the preparation of single and hybrid nanofluid. The SR, tool life, CF, and tool wear were studied. The tool wear, tool life and SR were having significant results on hybrid nanofluid condition [48]. The study cutting force, surface roughness in turning of graphene reinforced Al MMC in dry condition. For the experimental study, the RSM-CCD method was adopted. The results were analyzed through ANOVA and NSG 2. Feed rate was most influencing factor on both results. NSG 2 provides 10% error when compared with test results [49]. The 50% volume of aluminum and SiCp particles were reinforced to form Al MMC, which becomes a difficult-to-cut, hard, high strength and stiffness material. the DOE was applied for an experimental test to study tool life, SR and CF. The optimisation was done by the regression method and neuro-fuzzy logic methods. Higher cutting speed results in reduced CF, tool life and roughness [50].

AL 6063 was reinforced with groundnut shell, jute and sugarcane ash to prepare Al MMC material using stir casting material. The Taguchi's method was applied for machining to study SR. The RSM, GA, and ANOVA were used for optimisation. The GA results are very much significant with the results obtained by RSM [51]. An alternative to mineral oil-based cutting fluid was replaced by vegetable-based oil for machining operation to overcome harm to the environment and health. The turning of AISI 1040 was done with MQL coconut oil, dry, flood, and MQL mineral oil as cooling environments to study the flank wear, crater wear, temperature, and morphology. The study reveals the MQL-CO reduces the temperature at the contact zone and friction compared to other conditions of cooling [52].

The MQL cupric oxide nanofluid was used in the machining of AISI D2 material in turning. The SR, CF, flank wear and temperature were studied in hard turning under NFMQL, MQL, and dry conditions. RSM and DF were used for analysis of results. The feed was most effective over surface roughness, while both feed and depth have an effect over cutting force and power [53]. An integrated methodology of NSG 3 and Random Forest regression was used for optimisation of results. A vortex tube cooling and MLQ environment was used for turning of SKD 11 steel to study SR, and TW.

RAM BBD was used for experimental testing. The integrated methods exhibit better results [54]. The review of cooling fluid as vegetable oil in machining was done along with flank wear, SR, and the Temperature of the tool and CF. The review of FW, SR, and CF vs. Speed was collected. The worn tool has more roughness compared to new. There is no correlation between FW and SR [55]. The SiCp and aluminum metal matrix reinforcement was reviewed due to its applications. This material becomes hard to cut, which exhibits higher CF and FW. The review focused on the influencing factors. The main purpose of the review is to study the turning of MMC and parameters affecting tool wear and roughness. [56]. The review of the temperature zone at the contact of the tool tip and workpiece was done. The influence of high temperature affects FW, tool life and the surface of the workpiece. Also reviewed the methods of temperature measurements along with merits and demerits [57]. The study involves the investigation of the impact of parameters on cutting pressure and force, and roughness in the turning of EN-GJL-250. Si3N4 coated and uncoated inserts were used in turning with other input parameters. To determine the contribution of cutting parameters, ANOVA and LM, DT, SVM, and Da-DNN algorithms were used. The coating of inserts improves SR and reduces the force [58].

The turning of Inconel 718 material was used to study the wear, temperature, and tool life. The new approach of using a prototype toolholder and adjustable nozzle design with temperature measurement ability. The experiment reveals that the nozzle design has no effect over temperature. The passing of higher cutting fluid reduces the wear of the tool and gives longer tool life [59]. The study involves the controlling of CF, temperature, and energy consumption in dry turning of Ti6Al4V. The RSM and ANOVA were used for experiments to study wear and temperature. The depth of cut has the highest effect over CF and temperature. GRA was used for optimisation of cutting parameters [60]. The dry, MQL lubricant, and vortex cooling conditions were used in the turning of nickel-based Inconel 625 alloy. The CF, temperature, SR and tool life were studied as responses. The GRA was used to optimize the responses. The cooling effects reduce the wear and improve tool life [61]. The effect of the WC tool and HSS inserts was used in the turning of 304 austenite Steel. The flank wear was considered as a response in the study. RSM was used for analysis of response. The WC inserts provide better tool wear compared to HSS inserts [62].

The study focuses on turning SUS430C stainless steel because of its excellent corrosion resistance. The three responses, FW, SR, and MRR were optimized by NSG-2. The XG Boost model was validated by RSM BBD experimental data. The NSG 2 results exhibit better performance [63]. The AISI 316L steel was used in turning by using dry, MQL, NF MWCNT MQL cooling conditions. SR, feed force, and temperature were measured in the process as responses. The NF MQL provides better results. The NSG 2 was used for optimisation of models [64]. AISI 310S steel was used in turning by using dry, MQL vegetable oil, MQL $nMoS_2$, MQL nGP, MQL $nMoS_2$, and nGP conditions. NSG 2 and TOPOSIS were used for optimisation. MQL nGP exhibits better results compared to other conditions [65]. For optimisation of machining parameters, the NSG 2 VIKOR, and MOORA methods were used. The RSM was used for the experimental plan to turn AISI D3 steel to measure CT, CF MRR, and FW. The NSG2 and VIKOR exhibit better results of MRR [66].

Inconel 690 was machined in a dry, MQL, MQL NF, and CO_2 condition. Taguchi's array is used for experiment work. The ANOVA was used to examine the responses. The TLBO and NSG 2 were utilized for optimisation, of parameters. After successful optimisation the NSG 2 exhibits the best results compared to other [67]. The SR and tool wear were measured during CNC turning of AISI 316. The GA and PSO were used for optimisation of cutting parameters. A significant positive relationship was found during hybrid optimisation. The minimum Ra was produced [68]. In dry and HPC conditions the temperature and SR were measured during hard turning of 42CrMo4 steel. The MOGA was used to optimise the turning operation. The simultaneous minimization of both responses was done by MOGA [69]. The review of the cooking oil with all its properties are reviewed. The effect of cooking oil on surface roughness, tool wear, and MRR were reviewed with the effect of input factors [70]. The turning of SS304 steel was studied on roughness and wear by nano coolant as an additional parameter along with regular parameters. The effect of nano coolant was better than other responses [71]. The turning of titanium alloy by using different nanomaterials was studied. The graphene based nanofluids developed lower forces of cutting, roughness, and temperature [72]. The hybrid nanofluids were used in the turning of AISI4340 steel. A 0.75 CuO 0.25 Al_2O_3 combination performed well in the study of forces and roughness [73]. The LM 25 material was used in turning to study the cylindrical error, SR, and MRR by the grey relational analysis optimisation technique [74]. The A356 material is reinforced with bagasse ash in 2, 4, 6, and 8, wt percentages to study the mechanical properties [75]. The Al 6262 is reinforced with bagasse ash in 2% and 5% wt percentages. The prepared MMC was used in a study of mechanical properties [76]. The Al Si 10-Mg material is reinforced with sugarcane bagasse ash in 6%, 9%, and 12% by the stir casting process. The wear mechanism, morphology, and tensile properties were studied [77]. The Al6061 alloy is reinforced with 10% wt of SiC, and varying percentages of aloe vera ash and bagasse ash. 10% wt bagasse ash and 11% wt percentages aloe vera ash exhibit better compressive strength and hardness [78].

After reviewing the literature, the work on LM 25 aluminum is present but limited when compared with other

aluminum alloys, the LM 25 material is used for different machining processes but limited in the turning process [3, 5–9, 74]. In the literature, no specific research reveals any work on LM 25 material with selected reinforcement, which shows the research interest. The reinforcement of different nano materials with other aluminum alloys was studied. The combination of nano TiO_2, nano ZrO_2, and bagasse ash with LM 25 is not available from the literature [1–10, 75–78]. In a simple way, the research topic is selected to combine the industrial relevance of LM 25 with the economic benefits of low-cost bagasse ash utilization, while focusing on a clear research gap in the cast composite and sustainability literature.

The LM 25 material is deliberately selected as a base material in the study because of its castability and machinability characteristics. This material is having wide industrial utilization in the field of automotive and aerospace components, which creates the interest in this material study. The selected material with different hybrid nano material reinforcement provided the gain in hardness, tensile and compression strength. Compared to other wrought alloys, this material got less attention in the casting of composites with the combination of bagasse ash and nano reinforcement research. The above-discussed factors strengthen the novelty of focusing on LM 25 cast composites.

The PVD coated TiCN, Al_2O_3 coated carbide inserts are used in turning operations [1, 5, 8, 9]. The effect of coated inserts on temperature at the contact zone of insert and workpiece during turning is studied, and the cutting force is measured. In this research, the soybean oil, which is easily available and low cost, is utilised as a base fluid to develop nanocoolant. Because of its fatty nature, it helps in reducing the heat and friction at the contact area [29, 31, 33, 36]. The combination of 2 nanomaterial TiO_2, MoS_2 and the combination of 3 nanomaterial TiO_2, MoS_2, ZnO along with surfactant, is concentrated with soybean oil for the preparation of nanofluid and used as a minimum amount of coolant (MAC) [10–28].

The effect of cutting factors over responses is done by desirability function analysis (DFA), and response surface methodology (RSM) [4, 6, 42, 46, 49, 51, 53]. The optimisation provides the best parameter combination for superior finishing, MRR and reduced wear, temperature and cutting force and to establish mathematical models. The optimisation is also done by MATLAB algorithms [39, 49, 54, 68–70]. The multi objective genetic algorithm (MOGA), particle swarm optimization (PSO), non-dominated sorting genetic algorithm (NSG) MATLAB optimisation are used to get superior responses, and analysis of parameters are done by Pareto front simultaneous optimisation. The results are be compared with experimental tests. The simultaneous optimisation of MRR Vs SR, insert temperature, Flank wear, Z Force are inculcated from all three MATLAB optimisation techniques. In all the generated Pareto front graphs, the smallest values of SR, insert temperature, Flank wear, Z Force are obtained with higher MRR value in Pareto front graphs.

2 Selection of base material and method of composite fabrication

2.1 Material selection and A-HMMC preparation

The LM 25 material is selected as the base aluminum material for the study. It is a silicon aluminum-based alloy with better castability characteristics, high strength, and good resistance to corrosion in nature, with weldability nature shown in Fig. 1.a. Because of its characteristics the industries are using this material in the composite form in a wide variety of applications like marine, automobile, aerospace, and engine parts. The base material has a density of 2.68 g/cm^3 and the cast LM 25 has 57.44 HV micro-Vickers hardness, 213.6 MPa compressive strength, and 130–150 MPa tensile strength. The composition of LM 25 is shown in Table 1.

2.2 Selection of reinforcement materials

The characteristics of Al-HMMC depend on its reinforcement materials. The reinforcement materials are selected on their properties and their applications. The nano titanium dioxide (TiO_2) with 4.23 g/cm^3 density is a naturally available oxide with a high melting point, is selected as a filler material because of its hardness, corrosion and wear resistance. On adding leads to a stable microstructure, which adds the hardness, tensile strength and wear resistance as shown in Fig. 1.b. Another material nano Zirconium dioxide (ZrO_2) with 5.68 g/cm^3 density, is selected because of its high toughness and strength and improves the corrosion resistance in composites as shown in Fig. 1.c. Both filler materials have a 50 to 80 nm particle size. The bagasse ash consists of alumina and silica content, is used as another filler material, which helps in improving the composite strength, wear and hardness as shown in Fig. 1.d. The percentage of bagasse ash is kept constant and the other two nanofiller material are varied in production of Al HMMC [1–9].

2.3 Preparation of A-HMMC

The process of preparation of A-HMMC involved the stir casting method to fabricate a better-quality hybrid composite with uniform distribution of filler material without defects. The process of preparation of A- HMMC [1–3] by stir casting is represented in Fig. 2. At the beginning the LM 25 material ingot is cut into small pieces and placed inside the crucible. Later the crucible is placed inside the resistance furnace and

Fig. 1 Filler materials used for casting

Table 1 Chemical composition of LM 25

(Al) %	(Si)%	(Mg)%	(Fe)%	(Mn)%	(Ti)%	(Cu)%	(Ni)%	(Zn)%	(Pb)%	(Sn)%
91.3–93.3	6.5 to 7.5	0.2 to 0.6	0.5	0.3	0.2	0.1				0.05

Fig. 2 The stir casting process

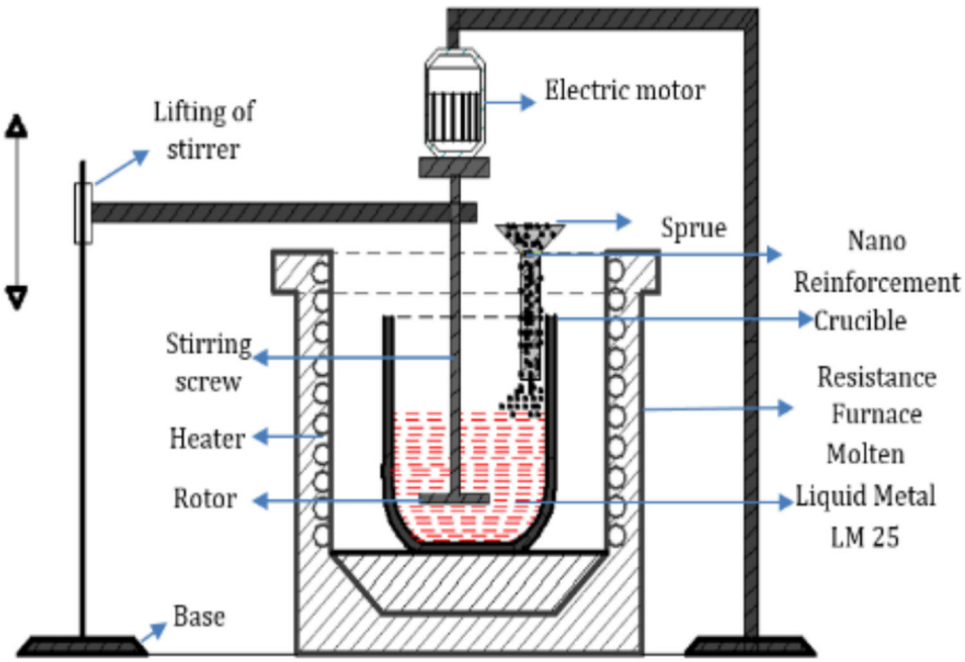

heated up to 690 °C to convert the LM 25 pieces into liquid form. The filler materials are preheated up to 250 oC for 60 min before adding to the crucible. The preheating process removes the moisture content from the filler material and also improves the wettability which helps in casting. The preheated filler materials are added into crucible through sprue, when the material in the crucible reaches the molten state.

The stirring of molten metal is done by a stirrer which is inserted inside the crucible. Molten metal is stirred during the adding of heat-treated filler material up to 500—1000 rpm. This helps in the uniform mixing of filler material and removes the defects of casting. After the stirring process is over, the molten metal is poured into the dies of 300 mm length and 25 mm diameter, then allowed to solidify. The three different weight percentage combinations for castings are shown in Table 2. composite M1—LM 25 84% + 3% $nTiO_2$ + 5% $nZrO_2$ + 8% bagasse ash composite M2—LM 25 84% + 4% $nTiO_2$ + 4% $nZrO_2$ + 8% bagasse ash, and composite M3—LM 25 84% + 5% $nTiO_2$ + 3% $nZrO_2$ + 8% bagasse ash. All three prepared compositions are represented in Fig. 3.

2.4 A-HMMC's microstructure study

The microstructural analysis of prepared A-HMMC is done by a 1000 × zoom metallurgical microscope. The microstructure study is required to check whether the filler materials distributed uniformly over the base material. Figure 4. shows

Table 2 Cast composition of A-HMMC

Sl. No	Samples Coding	Cast Compositions (Wt %)			
		LM 25	$nTiO_2$	$nZro_2$	bagasse ash
1	M1	84	3	5	8
2	M2	84	4	4	8
3	M3	84	5	3	8

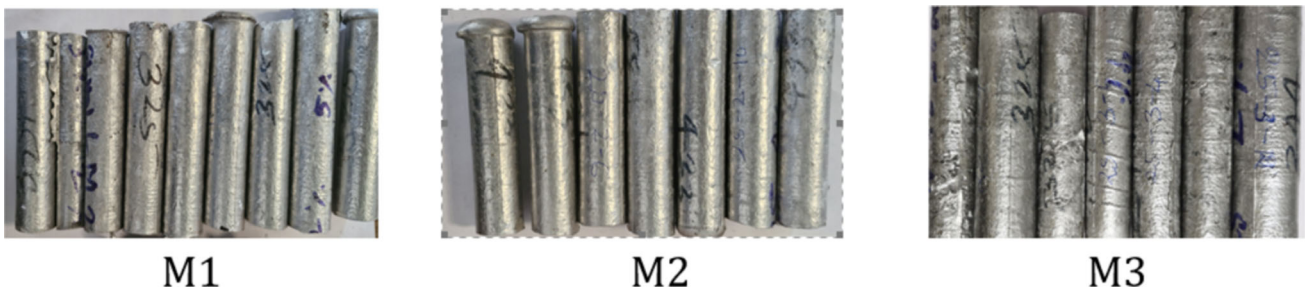

Fig. 3 Prepared three combinations of A—HMMC

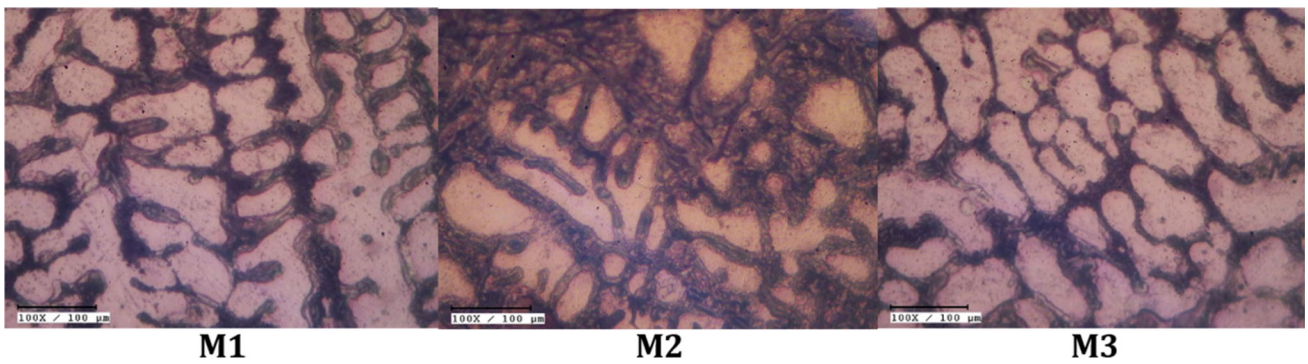

Fig. 4 The microstructure of prepared A-HMMC cast

the microstructure of all three prepared combinations of A-HMMC. To study the microstructure of the specimens, they have to be prepared by different steps. These steps involved the specimen being cut into the required height, during cutting, care is taken to avoid excessive heat and deformation on the surface where the image is to be captured. Then allowed for hot or cold mounting in a soft epoxy resin, the exposed surface is grinded and polished by SIC paper to obtain mirror-like scratch free finished surface. Followed by cleaning and chemical etching. Then the specimen is used to study microstructure.

The microstructure of prepared A-HMMC shows filler materials distributed uniformly over the base material. The inverted microscope is used for microstructural characterization, which is suitable for large specimens. The polished face of the specimen is placed above the light source to obtain a focused image of it. The microscope is equipped with a 5MP high-resolution camera to capture the image of the sample. The micro cam software helps to capture the structure of the sample surface.

2.5 Measurement of mechanical properties of fabricated A-HMMC cast

To check the quality of the fabricated composites, the hardness value, compression and tensile strength are measured in the study. Depending on the weight percentage of filler material used, the variation in properties of composites is observed. Compared to the properties of the base material, all three fabricated cast composites have improved properties. The measured mechanical properties of all cast composites are tabulated in Table 3. The density of composites is measured to determine the performance of composites and is measured by the principle of Archimedes. The density of base material LM 25 is 2.68 g/cm^3, the measured density of

Table 3 The mechanical properties of fabricated composites

Fabricated A-HMMC cast	Density gm/cm^3	Micro Vickers hardness HV	Tensile strength MPa	Compression strength MPa
M1	2.58	84.50	66	445.9
M2	2.59	90.55	98	467.6
M3	2.82	96.20	148	539.1

all three fabricated cast composites is very close to the density of the base material. This density plays a very important role in the study of wear.

The base aluminum material has 57.44 HV micro-Vickers hardness. The specimen of all three cast composites is prepared as per standard steps, and at three different places of each sample, the hardness value is measured, and the maximum hardness value is considered. The hardness values of fabricated composites varied from 84.5 HV to 96.2 HV. As compared to base aluminum the improvement in hardness is observed. The 3% $nTiO_2$ and 5% $nZrO_2$ have 84.5 hv which is the lowest in the fabricated cast. The 5% $nTiO_2$ and 3% $nZrO_2$ have 96.2 hv which is the highest in the fabricated cast. The bagasse ash weight percentage is kept at 8% constant for all composites. From the data of hardness, an increase in hardness value is observed when there is an increase in weight percentage of $nTiO_2$ and a reduction in weight percentage of $nZrO_2$. This indicates that the variation of filler material in the castings changes in the hardness value can be observed.

The specimens for tensile tests are prepared as per the ASTM standard for all three different cast composites. The measured values range from 66 to 148 MPa. The base material has 130 MPa tensile strength. In comparison, the M3 composite has higher tensile strength. The 5% $nTiO_2$ and 3% $nZrO_2$ and 8% bagasse ash exhibit the best tensile strength. As the increase in $nTiO_2$ percentage weight, the increase in tensile strength can be observed in the composition. The base material has 213.6 MPa compression strength. All the fabricated composites have compression strength more than the value of the base material. This improvement of compression strength is because of bagasse ash reinforcement in the A-HMMC, which is kept constant in all three composites. The 5% $nTiO_2$ composition has the highest compression strength at 539.1 MPa. All measured mechanical properties vs fabricated A-HMMC's in improvement order is represented graphically in Fig. 5.

3 Experimental conditions

3.1 Machining approach

In the industry the characteristics of machining are measured by quantitative measurable characters related to surface. During the turning process, the heat generated between the contact of the insert and the work surface is very high, and the cutting force generated due to input parameters is also high. This temperature and cutting force affect the surface characteristics in many ways. The insert used and the coating used for the insert plays a very important role in turning operations. The temperature and cutting force will develop at the area where the insert and workpiece contacts, the coating will reduce the temperature at the contact zone. If the temperature at the zone reduces, the flank wear of the insert will also reduce, and the life of the insert will be increased.

Now a days vegetable oil is used as cutting fluid in the turning process to overcome health issues and surface related issues in the industrial environments. From literature, the finishing and flank wear of the insert was better by using vegetable oil compared to conventional fluid used in the machining process. And also, the health-related issues were decreased. Further developments in cutting fluid research provide the knowledge of using nanomaterials with vegetable oil to prepare the nano fluids. The ground nut oil, palm oil, sunflower oil, soybean oil etc., were used as base oils to prepare nanofluid. The hardness of cast composites, and nano coolants are considered as input factors with speed and feed by keeping DOC constant to study the in-process responses like insert temperature and cutting force. After processing the roughness of the surface, flank wear, and MRR is recorded offline. The dry, PVD coated TiCN and Al_2O_3 coated carbide inserts are used in turning operations to check the performance of inserts.

3.2 Work material, cutting insert, and insert holder

The LM 25 aluminum hybrid composites in three different combinations are prepared in 300 mm length and 25 mm diameter. The nano titanium dioxide, nano zirconium dioxide and bagasse ash are used as reinforcements for the preparation. The prepared cast composites are cut into 100 mm lengths and 25 mm diameters and are used for the turning

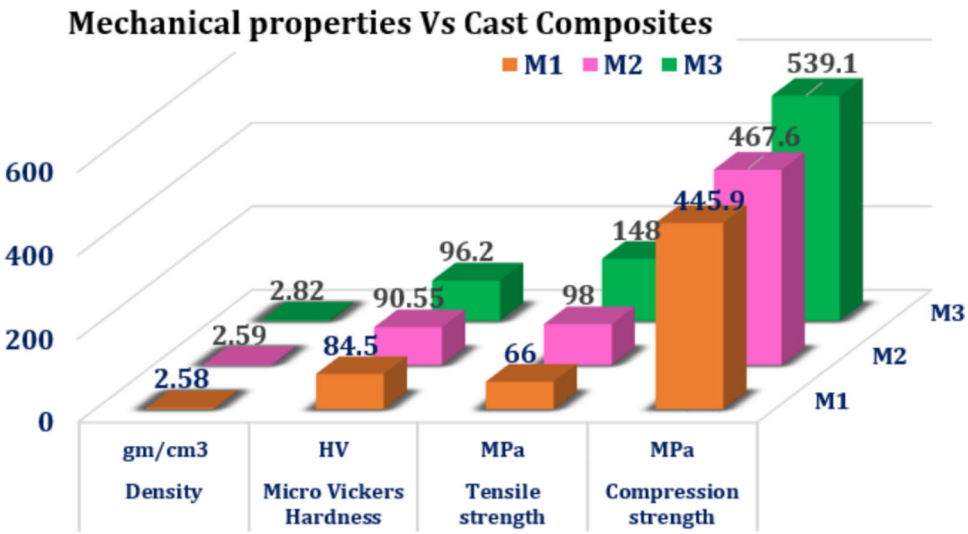

Fig. 5 Mechanical properties Vs Cast Composites

Fig. 6 The Inserts and Holder used in experimental work

process in each test. All three composite properties are tabulated in Table 3. The TNMG160408 G332 tungsten carbide inserts are selected for the turning operation. The shape of the inserts is triangular with 4.67 mm thickness, and the TNMG2020K16 insert holder is used. The inserts are silver coated and specially used to cut aluminium material as shown in Fig. 6.

3.3 Coating of inserts

The physical vapour deposition method is chosen for coating of inserts. This method involved the process of converting of solid material into vapour form in a vacuum and depositing it on the cleaned and degreased target surface [5, 8, 9]. The purpose of coating is to improve the wear resistance and hardness of inserts. Some of the inserts are used as uncoated, called as C1, some are coated with C2-TiCN which is a blue grey in colour and some are coated with C3-Al_2O_3 coating, which is a dark grey in colour, the coating, is done from Globus Engineering Solutions. The thickness of the coating is 4-microns with a single layer. The coating of inserts in turning operation is studied to overcome the temperature at the contact zone. If the temperature is high, the insert will wear at a faster rate, leading to a lower insert life. If the coated inserts were used the temperature at the contact zone will reduce and increase the insert life.

3.4 Nano coolant preparation

In the machining industries, the fluids used for cooling are in high volume flood conditions to remove heat at the contact of the tool and work. At present the effect of regular coolants in industries is becoming a very tedious issue, because it is affecting the environment as well as workers health. To overcome such issues, many researchers have proposed the use of nano coolant. This nano coolant is produced by using cooking oil as a base oil and very small quantities of nano particles are mixed with the base oil. These nano coolants are used in the minimum amount of coolant in machining to avoid wastage and be economical. In the view of such problems, the researchers have developed the nano coolants by using vegetable oils. The past researches [10–28] are proposing the results by using nano coolant are better in surface related and health issues. The hybrid nano coolants are recent developments in the research.

In the study the soybean oil [29, 31, 33, 36] is used as a base oil for the preparation of nano coolant. The base oil has 907 kg/m^3 density, 0.303 cm^2/sec kinematic viscosity, and a 489.2 °F flash point. The combination of 2 nano material TiO_2, MoS_2 and the combination of 3 nano material $nTiO_2$, $nMoS_2$, nZnO [71–74] along with CTAB surfactant 0.4 g is concentrated with soybean oil for the preparation of nano fluid and used as minimum amount of coolant (MAC). All nano materials varying from 50 to 100 nm particle size with

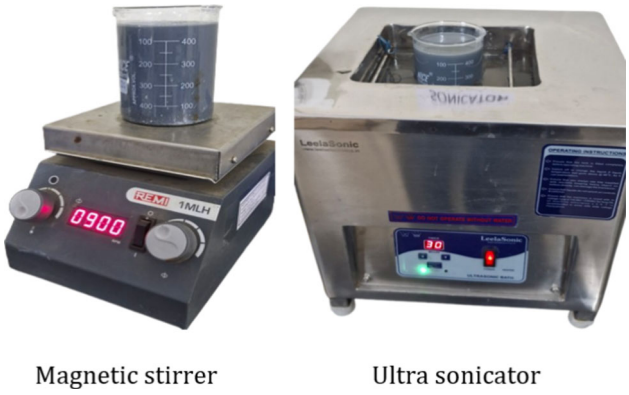

Fig. 7 Stirring and ultrasonication of nano coolant

99% purity are used to prepare nano coolant. The $nTiO_2$ is selected because of its heat transfer capabilities and lower temperature capabilities. The $nMoS_2$ is selected because of its low thermal conductivity and temperature stability. The nZnO is selected because of its heat removal and cooling effects.

The different weight percentages of nano materials are weighed from a digital weighing machine and concentrated with 100 ml of pure soybean oil. Nano coolant (NC) 1—1.0 weight % $nTiO_2$, 1.5 weight % $nMoS_2$, is concentrated with 100 ml of soybean oil and considered as one nano coolant. Nano coolant (NC) 2—1.0 weight % $nTiO_2$, 1.5 weight % $nMoS_2$, and 0.5 weight % of nZnO is considered as another nano coolant for the study. The CTAB helps in mixing of concentration without leaving the particles at the bottom. The 100 ml base oil is taken into a beaker, and slowly the nano particles are added with stirring. The concentration is stirred for 40 min by magnetic stirrer at 900 rpm on REMI 1MLH magnetic stirrer for proper mixing of nano particles in the base liquid. Followed by sonication, which passes the sonic waves to the concentration to avoid aggregation of particles at the bottom. The ultra sonication is done by Leela sonic for 30 min at 50 Hz frequency. The prepared nano coolant is used in minimum amount of coolant (MAC) condition after preparation. The stirring and sonication of concentration is shown in Fig. 7. The use of nano coolant helps in turning operation by reducing heat at the contact zone, and increasing insert life by reducing flank wear of the insert.

4 Experimentation outline

4.1 Cutting parameters and measuring apparatus

To investigate the effect of hybrid nano coolant in MAC condition and the insert coating in turning the process, the study is designed with four input factors. The four factors with three levels are speed (224, 499.5, 775), feed rate (0.159, 0.299, 0.44), LM 25 three cast composite hardness (84.5, 90.35, 96.2), and cooling condition (1-Dry, 2-NC-1, 3-NC-2) are considered for the experimental test by keeping the cutting depth constant at 0.3 mm for all experiments. The uncoating 1-C1, 2-C2-TiCN, and 3-C3-Al_2O_3 are used randomly in the process to study the insert flank wear for three different conditions. The response surface – BBD approach is used to obtain the combinations of factors to evaluate surface roughness (SR), flank wear (FR), insert tip temperature (T), Z cutting force (ZF), and volume of material removed (MRR). The experimental plan will be extracted from Taguchi's method. The Taguchi's method will give well defined combinations for testing. This can be done from MINITAB software by defining input factors, levels of parameters and responses. The parametric combinations of experimental tests planned are shown in Table 4.

Table 4 Parametric combinations of experimental tests

Factors	UNITS	LEVELS		
		1	2	3
Speed	rpm	224	499.5	775
Feed Rate	mm /rev	0.159	0.299	0.44
Material Hardness	HV	84.5	90.35	96.2
Cooling Condition	–	1	2	3

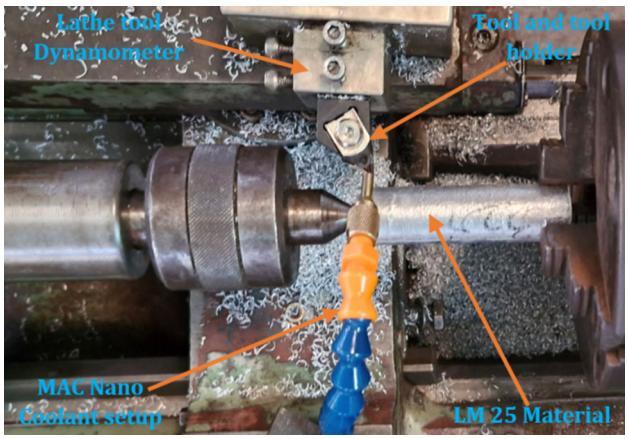

Fig. 8 Experimental and nano coolant setup

The experimental setup is shown in Fig. 8. The two responses are measured after the machining process. Surface roughness is measured using the SJ210 roughness measuring instrument at two different areas of the work piece and the average is taken as SR value. The wear of the flank (Vb max) is measured by inverted metallurgical microscope. The instrument has 1000 × zoom and software compatibility to capture the wear area by a 5MP camera. The wear area of the captured image is measured by the software tool. Two in

Table 5 Experimental plan and recorded responses

SI. No	Speed	FR	Material hardness	NC	Insert Coating	SR	MRR	Insert tip temp	IFW (V_b)	Z force
	rpm	mm/rev	VH	–	–	µm	mm^3/min	°C	mm	kgf
1	775	0.2995	90.35	3	3	6.391	4609.55	86.5	0.2255	2.8
2	499.5	0.44	96.2	2	2	10.289	3643.14	74.58	0.0142	7.0
3	499.5	0.159	96.2	2	2	4.8366	3086.18	42.9	0.0587	3.0
4	499.5	0.159	90.35	3	2	4.71189	4253.15	49.7	0.1155	2.0
5	224	0.2995	90.35	1	1	9.283	3184.72	68.76	0.2055	5.8
6	499.5	0.2995	96.2	1	2	9.09	2746.37	54.21	0.1457	6.0
7	499.5	0.2995	90.35	2	2	7.921	4119.53	43.2	0.1987	4.0
8	499.5	0.2995	96.2	3	2	7.35152	3191.61	61.21	0.1193	5.9
9	224	0.159	90.35	2	1	3.296	3861.61	44.5	0.0781	1.4
10	775	0.44	90.35	2	3	7.378	4635.79	71.26	0.1384	5.0
11	224	0.2995	84.5	2	1	6.529	3308.01	60.8	0.1666	4.0
12	775	0.159	90.35	2	3	4.395	4312.16	48.1	0.1532	1.0
13	499.5	0.2995	90.35	2	2	7.27145	4151.51	54.7	0.1925	4.0
14	499.5	0.159	84.5	2	2	4.643	3814.04	53.2	0.0348	2.8
15	224	0.2995	90.35	3	1	6.223	4078.68	47	0.2817	4.0
16	499.5	0.2995	84.5	1	2	8.27124	2551.67	49.7	0.3231	9.4
17	775	0.2995	90.35	1	3	7.196	3377.5	46.9	0.4151	6.0
18	499.5	0.44	90.35	1	2	10.6804	3701.61	50.7	0.2687	10.0
19	499.5	0.159	90.35	1	2	6.65035	3303	38.47	0.245	5.0
20	499.5	0.2995	84.5	3	2	6.68903	4205.09	63.1	0.2673	4.0
21	224	0.2995	96.2	2	1	6.844	3200.94	69.07	0.0277	5.0
22	499.5	0.44	90.35	3	2	8.96966	4583.75	79.8	0.3592	6.0
23	224	0.44	90.35	2	1	9.68706	4232.3	83.3	0.1379	5.5
24	775	0.2995	96.2	2	3	7.6	3267.71	72.48	0.0493	4.2
25	499.5	0.44	84.5	2	2	7.303	3806.09	73.8	0.1828	6.9
26	499.5	0.2995	90.35	2	2	7.9	4190.61	57.62	0.1918	4.0
27	775	0.2995	84.5	2	3	5.98829	4169.14	78.8	0.1020	5.0

process responses are recorded, and the insert tip temperature is measured by the Pti120 thermal imager. The temperature image is captured at the highest value in all experiments are recorded in degree Celsius as a response. The feed force in the Z direction is recorded by the lathe dynamometer UIL 15 model in kgf. The experimental plan with recorded responses is presented in Table 5.

The insert wear is observed at the place where the contact of inserts and workpiece area occurs. At the contact area, due to variable regular parameters, the heat generation is high, due to this the wear of inserts takes place. This flank wear reduces the life of inserts and damages the dimensional accuracy of the workpiece contact area. The flank wear of insert $V_b > 0.3$ mm is allowable when the surface is even. If the surface is uneven $V_{b\,max} > 0.6$ is followed. The tool life criteria are followed in the study. In the turning of each experiment, fifteen cuts are considered irrespective of cutting combinations with variation in cutting time.

The material removal rate (MRR) is evaluated by Eq. 1 [37].

$$MRR = \frac{\mathrm{Wi}_x - \mathrm{Wi}_y}{\mathrm{Ti} * \rho} \quad \text{in milli meter}^3\text{/minutes} \tag{1}$$

$\mathrm{Wi_x}$ = Weight of w/p before turning (kg). $\mathrm{Wi_y}$ = Weight of w/p after turning (kg). Ti = completion time of one experiment (min). ρ = cast material density (kg/mm^3).

4.2 Effect of speed with responses on cast material

The evaluation of roughness value, wear of insert, and Z feed force by three different speed conditions. These responses are studied over three cooling environment, dry,

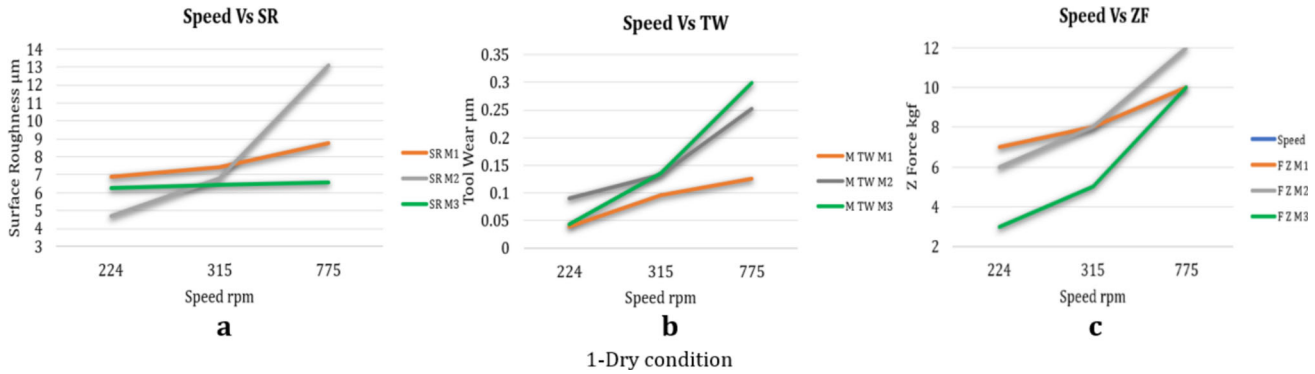

Fig. 9 Effect of responses with speed in dry condition

Nano Coolant—1, and Nano Coolant—2 conditions for all three-cast composites. In dry condition the uncoated silver colour inserts are used to measure the insert wear. The lowest insert wear for the M1, M2, and M3 composites is 0.0334 mm at 224 rpm, 0.0532 mm at 775 rpm, and 0.0338 mm at 224 rpm respectively. In dry condition, cast composite M2 has the highest roughness value of 13.08 µm at 775 rpm and the lowest roughness value of 4.7 µm at 224 rpm. M3 composite has higher insert wear (0.2987 mm at 775 rpm), M1 composite has the lowest insert wear (0.0387 mm at 224 rpm). The M2 composite exhibits 12 kgf force at 775 rpm, whereas M3 have very lowest 3 kgf force at 224 rpm. In comparison, the roughness value, wear of insert, and Z feed force increase with an increase in speed. The graphical representation of speed vs responses for all three composites is represented in Fig. 9. a, b, c.

In NC 1 condition, the lowest insert wear for M1, M2, and M3 composites is 0.0528 mm at 775 rpm, 0.2207 mm at 224 rpm, 0.1109 at 224 rpm respectively. The cast composite M1 has higher 9.23 µm at 224 rpm and lowest roughness value 5.76 µm at 775 rpm. The M2 composite has higher insert wear (0.626 mm at 775 rpm), M1 composite has the lowest insert wear (0.0604 mm at 224 rpm). The M1 composite have exhibits 6 kgf at 775 rpm force, whereas M3 have very lowest 1 kgf force at 224 rpm. In comparison the roughness value varied with respect to speed, wear of insert, and Z feed force increases with increase in speed. The graphical representation of speed vs responses for all three composites is represented in Fig. 10 a, b, c.

In the NC 2 condition, the lowest insert wear for the M1, M2, and M3 composites is 0.0323 mm at 224 rpm, 0.0211 mm at 224 rpm, and 0.0213 at 315 rpm, respectively. The cast composite M2 has a higher 11.25 µm at 224 rpm, and M2 has the lowest roughness value of 3.78 µm at 775 rpm. The M1 composite have higher insert wear (0.1352 mm at 775 rpm), M2 composite has the lowest insert wear (0.0241 mm at 224 rpm). The M2 composite exhibits 6 kgf at 775 rpm force, whereas M3 has the very lowest 2 kgf force at 224 rpm. In comparison, the roughness value varied with respect to speed, wear of insert, and Z feed force increases with the increase in speed. The graphical representation of speed vs responses for all three composites is represented in Fig. 11 a, b, c.

In comparison of the cast composition, the effect of surface roughness by speed on composite M2 material has the highest SR value of 9.23 µm at 224 rpm, and M2 has the lowest roughness value of 3.78 µm at 775 rpm. The effect of insert wear by speed on composite M2 have higher insert wear 0.626 mm at 775 rpm, and composite M2 has the lowest insert wear 0.0211 mm at 224 rpm, which is coated by TiCN. The effect of feed force Z by speed on composite M2 has the highest force of 12 kgf at 775 rpm, and M3 has the very lowest of force 1 kgf at 224 rpm. The M2 composite material has better properties.

In comparison of the cast composition, the M3 material shows the improvement in mechanical properties. Hence the M3 material is considered for the evaluation of responses in different cooling environments. The evaluation of roughness value, wear of insert, and Z feed force by three different speeds is conducted. The responses are studied over hybrid and single cooling environments, dry, Nano Coolant—1, Nano Coolant -2, $nTiO_2$, $nMoS_2$, and nZnO coolants in MAC conditions. Figure 12. a show the graph of Speed vs SR. The Nano Coolant -2, shows the better performance in comparison with others. Figure 12. b shows the graph of Speed vs Z Force. The Nano Coolant -1, shows the better performance in comparison with others by least values of forces in all speed condition. Figure 12. c shows the graph of Speed vs TW. The Nano Coolant -1, shows the better performance in comparison with others by least values of tool wear in all speed conditions.

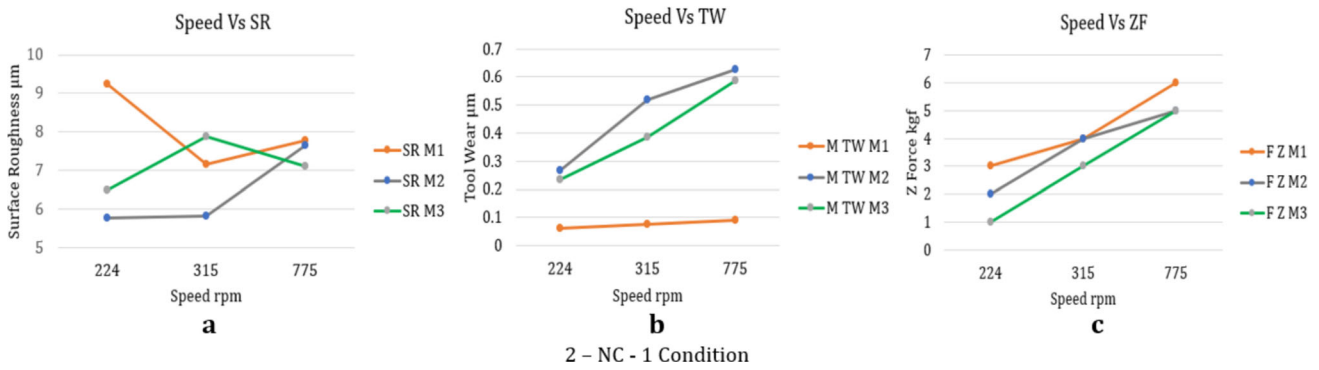

Fig. 10 Effect of responses with speed in NC—1 condition

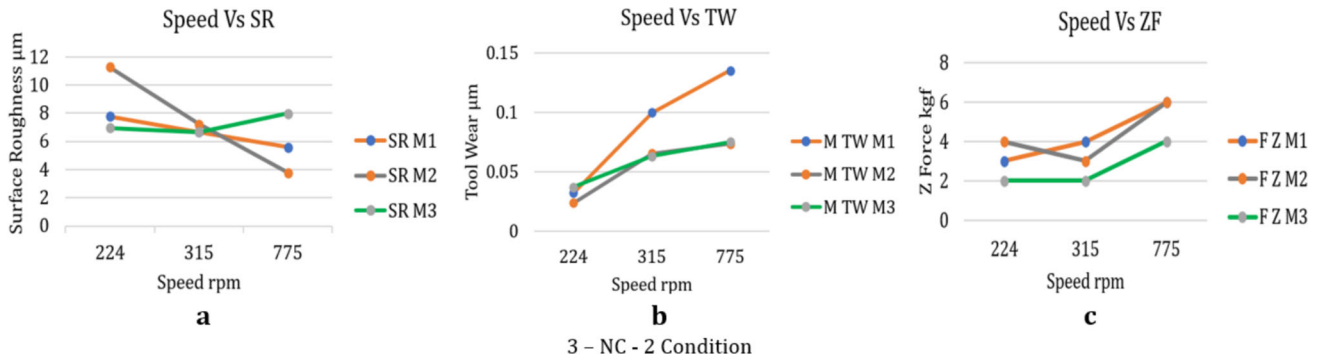

Fig. 11 Effect of responses with speed in NC—2 condition

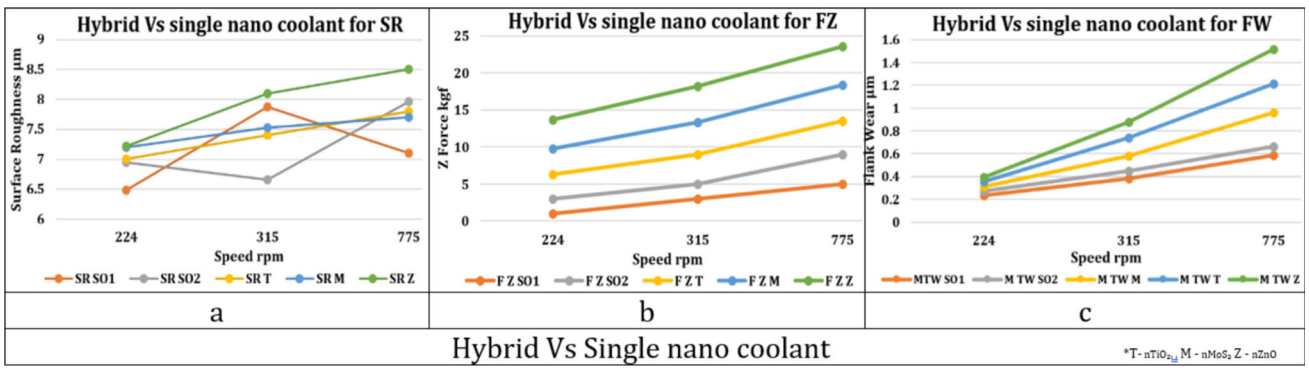

Fig. 12 Comparative graphs showing hybrid vs. single nano coolant

5 Data analysis and optimisation methods

5.1 Analysis by DFA

This is one of the most used multiple output data analysis techniques. This statistical technique provides the most significant parameter from a set of experimental data by response analysis. The desirability data is evaluated by converting responses into non-unit values [53, 58, 66]. This process involves two steps; the responses are transformed into desirability index (I_d.) separately. The I_d values varied between zero and one. In the next step, composite desirability (D_c) is developed by adding responses separately into a function. This process is carried out by the weighted geometric mean of all I_d values. The optimal parametric values are obtained from the maximum values of composite desirability (D_c). the value of composite desirability (D_c) becomes zero, this is not accepted.

5.1.1 DFA Optimization technique

Higher the value is better

$$I_d = \left(\frac{V_y - V_{\text{mini}}}{V_{\text{maxi}} - V_{\text{mini}}}\right)^x V_{\text{mini}} \le V_y \le V_{\text{maxi}},\ r \ge 0,\ 1,\ V_y \ge V_{\text{mini}},\ 0,\ V_y \le V_{\text{mini}} \quad (2)$$

Lower the value is better

$$I_d = \left(\frac{V_y - V_{\text{maxi}}}{V_{\text{mini}} - V_{\text{maxi}}}\right)^x V_{\text{mini}} \le V_y \le V_{\text{maxi}},\ r \ge 0,\ 1,\ V_y \le V_{\text{mini}},\ 0,\ V_y \ge V_{\text{mini}} \quad (3)$$

V_y = the output values, V_{mini} = lowest value of y^{th} output, V_{maxi} = highest value of y^{th} output. Separate desirability index I_d is evaluated by Eqs. 2 and 3, depending higher the better or lower the better response characteristics. When $V_y \ge V_{\text{maxi}}$, a I_d value equal to 1 condition is desirable. When $V_y \le V_{\text{mini}}$ I_d value is not desirable when its value is zero. Hence, the I_d values lie between one and zero.

The D_c composite desirability function is evaluated by Eq. 4.

$$CD(\text{Dc}) = \left(\text{Dc}_1^{x1} * \text{Dc}_2^{x2} * \text{Dc}_3^{x3} \ldots\ldots\right)^{\left(\frac{1}{l}\right)} \quad (4)$$

where, the responses are denoted by l. $D_{c\,1}$, $D_{c\,2}$, $D_{c\,3}$…. Denotes indexes of individual desirability. x_1, x_2, x_3…. denotes weights of responses. All output responses have same weightage. x_1, x_2, x_3, $x_4 = 0.5$ is considered in Eqs. 2 and 3.

The analysis of responses by DFA tabulated in Table 6. In CD column the largest value provides the rank one for DFA, as the lowest is last rank. In Table 6, 0.7013 is the largest CD value with experiment no. 01 is given as rank 1. The 775-rpm speed, 0.2995 mm/rev feed rate, Al_2O_3 coated inserts and NC 2 coolant are effective parameters to obtain best responses for cast material M2.

5.2 Data analysis by RSM

The response surface data analysis technique provides the interrelationship between responses and parameters. This relationship is developed using statistical software by providing different independent variables and their levels as input. The different cutting conditions are extracted from software, and experimental tests are conducted. The BBD design is inculcated in this research for experimental investigation. The observed responses are recorded and used for optimisation through analysis by ANOVA. This analysis develops a model for each response by analyzing the independent variables to study the significant effect. It will predict the independent variables for expected results [52, 54].

The predicted RSM variables are tested for experimental work to measure the responses and confirmation. The developed models indicate the relation between experimental conditions and measured outputs. The speed, feed rate, cast composite hardness, and cooling environments are used as independent cutting inputs. The SR, MRR, insert temperature, insert flank wear (V_b) and Feed force are measured as dependent variables.

Dependent variables are denoted by D and the independent cutting inputs is denoted by P. The relation between D and P is given by [56].

$$\text{P} = \text{D(speed, feed rate, cast composite hardness, and cooling environments)} \quad (5)$$

The RSM second order response model is given by:

$$P = y_o + \sum_{i=1}^{z} y_i Q_i + \sum_{i=1}^{z} a_{\text{ii}} Q_i^2 + \sum_{i,j}^{z} Q_i Q_j \quad (6)$$

y_o – Regression constant value, The linear, and quadratic terms—y_1, $y_2 \ldots y_z$ and y_{11}, $y_{22} \ldots y_{zz}$,

y_{12}, $y_{13} \ldots y_{z\text{-}1}$ are interaction terms. Q_1, Q_2, Q_3…… independent cutting inputs.

5.2.1 RSM optimisation

The statistical RSM-BBD design is used to study the independent cutting factors over SR, MRR, insert temperature, insert flank wear (V_b) and feed force in the turning of prepared cast composites. The numerical parameters denoted in the RSM regression equations are speed (× 1), feed rate (× 2), cast composite hardness (× 3), cooling environments (× 4) with three different levels. Table. 5. is the representation of developed experimental combinations through statistical software called Design Expert. Later the responses are used in the software for analysis to develop the RSM regression models.

5.2.2 RSM equation for material removal rate

$$MRR = 154731 + 4.80937 * x(1) - 9103.23136 * x(2) - 3480.55345 * x(3) + 3304.35201 * x(4) - 0.303950 * x(1) * x(2) - 0.047533 * x(1) * x(3) + 0.306795 * x(1) * x(4) + 77.38248 * x(2) * x(3)$$

Table 6 Computed desirability function analysis

Responses I_d values						CD	RANK
Si No	SR μm	MRR mm^3/min	Insert tip Temp ^oC	IFW (V_b) mm	Z Force kgf		
1	0.7622	0.9937	1.0000	0.7260	0.8944	0.7013	1
2	0.2302	0.7237	0.8671	0.0000	0.5774	0.0000	23
3	0.8896	0.5064	0.3037	0.3332	0.8819	0.2005	21
4	0.8990	0.9035	0.4835	0.5027	0.9428	0.4315	9
5	0.4350	0.5511	0.7941	0.6908	0.6831	0.2997	16
6	0.4641	0.3056	0.5725	0.5727	0.6667	0.1761	22
7	0.6113	0.8673	0.3138	0.6784	0.8165	0.3036	15
8	0.6714	0.5541	0.6881	0.5120	0.6749	0.2974	17
9	1.0000	0.7928	0.3543	0.3992	0.9775	0.3311	14
10	0.6687	1.0000	0.8263	0.5566	0.7454	0.4788	4
11	0.7498	0.6024	0.6818	0.6166	0.8165	0.3938	11
12	0.9226	0.9191	0.4478	0.5888	1.0000	0.4728	5
13	0.6794	0.8761	0.5813	0.6669	0.8165	0.4341	6
14	0.9042	0.7783	0.5538	0.2267	0.8944	0.2811	18
15	0.7769	0.8560	0.4214	0.8169	0.8165	0.4323	7
16	0.5712	0.0000	0.4835	0.8778	0.2582	0.0000	23
17	0.6869	0.6295	0.4189	1.0000	0.6667	0.3475	13
18	0.0000	0.7428	0.5046	0.7968	0.0000	0.0000	23
19	0.7388	0.6004	0.0000	0.7588	0.7454	0.0000	23
20	0.7352	0.8907	0.7161	0.7946	0.8165	0.5516	2
21	0.7208	0.5582	0.7982	0.1835	0.7454	0.2096	20
22	0.4813	0.9874	0.9276	0.9277	0.6667	0.5222	3
23	0.3668	0.8980	0.9661	0.5555	0.7071	0.3535	12
24	0.6459	0.5861	0.8415	0.2959	0.8028	0.2751	19
25	0.6763	0.7758	0.8577	0.6485	0.5869	0.4138	10
26	0.6136	0.8868	0.6314	0.6656	0.8165	0.4321	8
27	0.7971	0.8810	0.9163	0.4680	0.7454	0.4738	5

$$
\begin{aligned}
&- 121.00611 * x(2) * x(4) - 17.67059 * x(3) * x(4) \\
&- 0.000141 * x(1)^2 + 5758.21301 * x(2)^2 \\
&+ 19.66842 * x(3)^2 - 317.09560 * x(4)^2; \qquad (7)
\end{aligned}
$$

5.2.3 RSM equation for surface roughness

$$
\begin{aligned}
\mathrm{SR} = {} & -166.66827 + 0.022070 * x(1) \\
& + 9.07253 * x(2) + 3.68281 * x(3) \\
& - 2.85022 * x(4) - 0.022011 * x(1) * x(2) \\
& - 0.000100 * x(1) * x(3) + 0.002046 * x(1) * x(4) \\
& + 0.367562 * x(2) * x(3) + 0.405140 * x(2) * x(4) \\
& - 0.012566 * x(3) * x(4) - 0.000011 * x(1)^2 \\
& - 29.85835 * x(2)^2 - 0.020189 * x(3)^2 \\
& + 0.493980 * x(4)^2 \qquad (8)
\end{aligned}
$$

5.2.4 RSM equation for insert tip temperature

$$
\begin{aligned}
Temperature = {} & -577.81241 - 0.004991 * x(1) \\
& - 58.48504 * x(2) + 15.37784 * x(3) \\
& - 42.82014 * x(4) - 0.101013 * x(1) * x(2) \\
& - 0.002137 * x(1) * x(3) + 0.055681 * x(1) * x(4) \\
& + 0.939432 * x(2) * x(3) + 31.79715 * x(2) * x(4) \\
& + 0.133944 * x(3) * x(4) + 0.000133 * x(1)^2
\end{aligned}
$$

$$+ 84.45097 * x(2)^2 - 0.085793 * x(3)^2 - 0.115417 * x(4)\text{^}2; \quad (9)$$

5.2.5 RSM equation for insert flank wear

$$\begin{aligned}\text{Flank wear} = {} & 29.42740 - 0.000974 * x(1) \\ & + 1.57218 * x(2) - 0.641268 * x(3) \\ & - 0.502587 * x(4) - 0.000482 * x(1) * x(2) \\ & + 0.000018 * x(1) * x(3) - 0.000241 * x(1) * x(4) \\ & - 0.007553 * x(2) * x(3) + 0.391338 * x(2) * x(4) \\ & + 0.000504 * x(3) * x(4) - 1.94136 * x(2)^2 \\ & + 0.003516 * x(3)^2 + 0.109798 * x(4)^2; \quad (10)\end{aligned}$$

5.2.6 RSM equation for Z feed force

$$\begin{aligned}\text{Z Force} = {} & -94.75751 + 0.019051 * x(1) \\ & + 5.25409 * x(2) + 2.43439 * x(3) \\ & - 11.78487 * x(4) - 0.001076 * x(1) * x(2) \\ & - 0.000177 * x(1) * x(3) - 0.001361 * x(1) * x(4) \\ & + 0.057936 * x(2) * x(3) - 1.77936 * x(2) * x(4) \\ & + 0.051893 * x(3) * x(4) + 14.13028 * x(2)^2 \\ & - 0.014272 * x(3)^2 + 1.67477 * x(4)^2; \quad (11)\end{aligned}$$

The statistical R^2 value developed by RSM regression equations indicates how close the relation of responses is with the independent variables. The R^2 values of responses are SR (96.19%), MRR (94.3%), Insert Temperature (91.2%), Insert Flank Wear (V_b) (90.97%) and Feed force (90.23%). These percentages indicate the models developed are adequate.

5.3 Multi objective GA

Multi-objective GA is a matlab optimisation technique which is used to generate optimal factors for the desired responses. This technique has many steps to generate Pareto results. In the research, MOGA is utilised to study, the lower the better response and the higher the better response values at the same point on the generated graph. To obtain best solutions, the upper and lower bonds of all responses have to be defined. Followed by population type and size, where the required size has to be defined. The size of the tournament is used as 2. Then the constraint dependent mutation function with crossover is updated. Then the stopping criteria is defined to get refined results [68, 69]. The optimisation application is used from matlab software to generate data.

5.4 Multi objective PSO

MOPSO is also a matlab optimisation technique which is applied to optimise machining parameters to reduce the cost of manufacturing. The bird's velvet pattern theory is used to develop PSO algorithm, which is developed by Kennedy & Eberhard. The basic steps are that the particle initialization is defined by its velocities and positions. Followed by calculation of the objective function of each particle and comparing the particles with solutions. The above steps are repeated till the maximum iterations are reached. The results are generated through Pareto solutions to determine the best parameters. After getting the best particles, the distances relative to other particles are recorded in the particle's memory. In each iteration the global solution is recorded in the global best memory. To accelerate the particles in the direction of the best particles and global best inertia weight method is incorporated. The inertia weights are randomized between 0.1 to 1.1. This process enables maximum search space for solving many complex problems [39, 68].

5.5 Multi objective NSG II

It is a non-dominated sorting algorithm, which is used to solve many difficult industrial machining problems by optimizing different factors. The most effective Pareto front solutions are generated by the non-dominated sorting method. This method of sorting involves a generation of random populations followed by selection of crowded tournament selection with combining parent solutions called crossover followed by mutation. The generated offspring and parent populations are combined into a single population. On the basis of Pareto front principle, the combined populations are sorted into a non-dominated number of fronts. Distance of crowding is calculated for each sorted front. The parent population is developed from the sorted front by terminating [63–67].

In the initialization step, define the decision variables with minimum and maximum ranges. The objective functions are selected from the regression equations developed in the RSM. Then the objective function should be bifurcated as highest output or lowest. In the beginning, a random population is initiated for a specified size N within the constraints range, the developed parent population Q_t is evaluated through the objective. In the next step the sorting of the developed population is made into different non dominated fronts. In the first front, the best solutions were obtained, which are not dominated by any other individual population. In subsequent fronts the removal of solutions from the last dominated fronts

further finds the next non-dominated fronts. The fitness values are calculated for all Q_t values. The further step continued with the calculation of the crowding distance of each front of individuals. A higher distance is preferred as it helps in maintaining diversity in population and to avoiding clustering of solutions. In the next step, a selection of tournaments is made for generating the non-dominated rank. Which is followed by crossover, which combines two parental solutions to create new offspring. Mutation randomly alters the genes within a single solution. Repeat the process or terminate the process depending on the number of satisfactory iterations.

6 Results and discussion

6.1 Evaluation of parameters effect by DFA

The mean effect on CD values for all levels is tabulated in the Table 7. The optimal settings of all parameters are highlighted in the respective column of table. The optimal cutting condition in all levels is given by S3FR2CH2CE3, which is gathered from Fig. 13. The optimal settings are highlighted in the fig by red dash circle. The 775-rpm speed, 0.299 mm/rev feed, M2 cast composite, and three nano particle concentration coolants are the best optimal parameters to observe better responses. This setting is available in the experimental combination hence, the responses are 6.391 μm roughness, 4609.55 mm3/min MRR, 86.5 insert temperature, 0.2255 mm insert flank wear (V_b), and 2.8 kgf force.

6.2 Analysis of responses data by RSM

6.2.1 Surface roughness analysis

The regression of RSM's surface roughness with speed, FR, hardness of cast composites, and cooling environment is tabulated in Table 8. In the research, the ANOVA analysis is done by design expert software considering a confidence level of 90 percent. This method is applied to check the developed model's significance and the parameters effect on surface roughness. In the P column, the lowest values indicate statistical significance for the response SR.

In Fig. 14 the residuals of statistical analysis by ANOVA follow the recorded values of response SR. The values of residuals are scattered around the zero-line indicating the model is adequate. The distribution of residuals is not showing any inappropriate pattern. The values are very close to each other; hence, the model developed for SR is significant. Figure 15 represents the relationship between SR and the parameters of the 3D surface plot. Providing the variation in roughness values by varying the feed and speed. By increasing the feed rate the value of SR is increased continuously at the lowest speed. The lowest 3.296 μm SR is observed at 0.15 mm/rev feed and 224 rpm speed. This lowest value is recorded for M2 cast material and NC-1 cooling environment.

6.2.2 MRR analysis

The regression of RSM's MRR with speed, FR, hardness of cast composites, and cooling environment is tabulated in Table 9. In the research, the ANOVA analysis is done by design expert software considering a confidence level of 90 percent. This method is applied to check the developed model's significance and the parameters effect over MRR. In the P column, the lowest values indicate statistical significance for the response MRR. In Fig. 16 the residuals of statistical analysis by ANOVA following the recorded values of response MRR. The values of residuals are scattered around the zero-line indicating the model is adequate. The distribution of residuals is not showing any inappropriate pattern.

Figure 17 represents the relationship between MRR and parameter's 3D surface plot. Providing the variation in volume of material removed by varying the feed and speed. By increasing the feed rate and speed the value of MRR is increased continuously. The highest MRR is observed at 0.44 mm/rev feed and 775 rpm speed. This highest value is recorded for M2 cast material and the NC-1 cooling environment.

6.2.3 Insert tip temperature analysis

The regression of RSM's tip temperature with speed, FR, hardness of cast composites, and the cooling environment is tabulated in Table 10. In the research, the ANOVA analysis is done by design expert software considering a confidence level of 90 percent. In the P column, the lowest values indicate statistical significance for the response Insert tip temperature. In Fig. 18 the residuals of statistical analysis by ANOVA following the recorded values of response tip temperature. The values of residuals are scattered around the zero-line indicating the model is adequate.

Figure 19 represents the relationship between tip temperature and the parameters of the 3D surface plot. Providing the variation in tip temperature values by varying the feed and speed. By increasing the feed rate and speed the value of the tip temperature increased continuously. The lowest tip temperature is observed at 0.15 mm/rev feed and 499.5 rpm speed. This lowest value is recorded for M2 cast material and the NC-1 cooling environment.

6.2.4 Insert flank wear (Vb) analysis

The regression of RSM's Insert flank wear with speed, FR, hardness of cast composites, and cooling environment is

Table 7 Means response of parameters effect by DFA

Levels	Speed rpm	Feed Rate mm/rev	Cast Hardness VH	Cooling environment
1	0.3367	0.2862	0.3523	0.1372
2	0.2511	**0.3499**	**0.3662**	0.3288
3	**0.4582**	0.2947	0.1931	**0.4894**
Effect	0.2071	0.0637	0.1731	0.3521
Rank	2	4	3	1

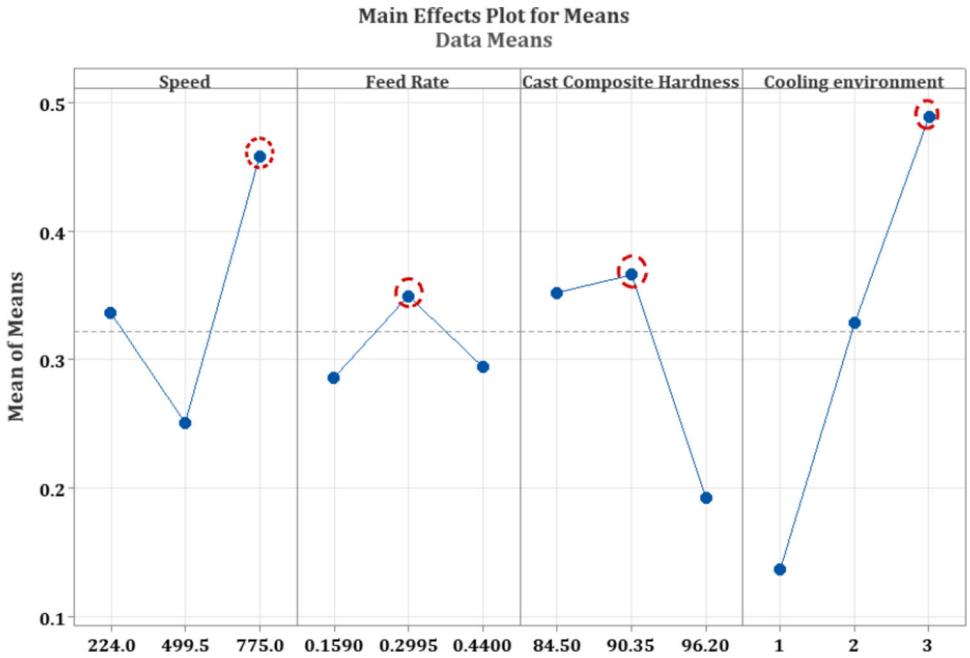

Fig. 13 Optimal settings of all parameters (S3FR2CH2CE3)

Table 8 Influence of parameter's effect over SR

Source	SS	DF	MS	F-value	p-value	
Model	83.56	14	5.97	21.63	0.0001	significant
A–x (1)	0.2288	1	0.2288	0.8288	0.3805	
B-x (2)	33.35	1	33.35	120.83	0.0001	significant
C-x (3)	2.46	1	2.46	8.91	0.0114	significant
D-x (4)	6.30	1	6.30	22.82	0.0005	significant
AB	2.90	1	2.90	10.52	0.0070	
AC	0.1829	1	0.1829	0.6626	0.4315	
AD	1.27	1	1.27	4.61	0.0530	significant
BC	0.6389	1	0.6389	2.31	0.1541	
BD	0.0130	1	0.0130	0.0470	0.8321	
CD	0.0378	1	0.0378	0.1370	0.7177	
A^2	3.79	1	3.79	13.74	0.0030	significant
B^2	1.85	1	1.85	6.71	0.0236	significant
C^2	2.04	1	2.04	7.38	0.0187	significant
D^2	1.30	1	1.30	4.72	0.0507	significant
Lack of Fit	3.04	10	0.3040	2.23	0.3490	
Pure Error	0.2725	2	0.1362			
Total	86.87	26				

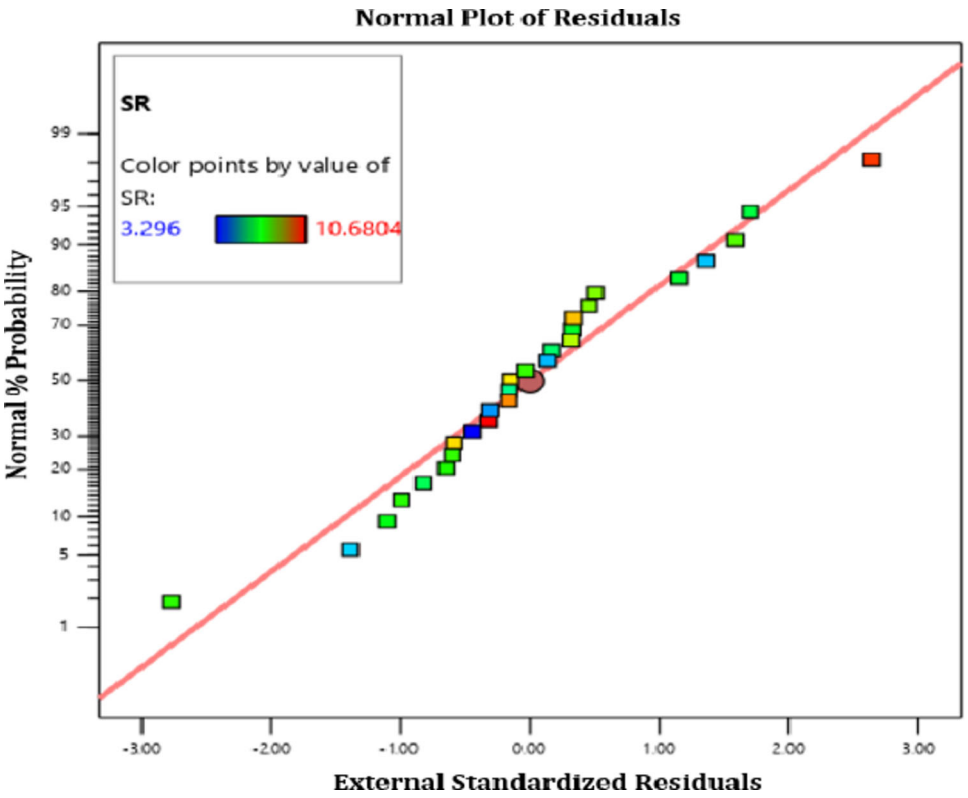

Fig. 14 Residuals plot for SR

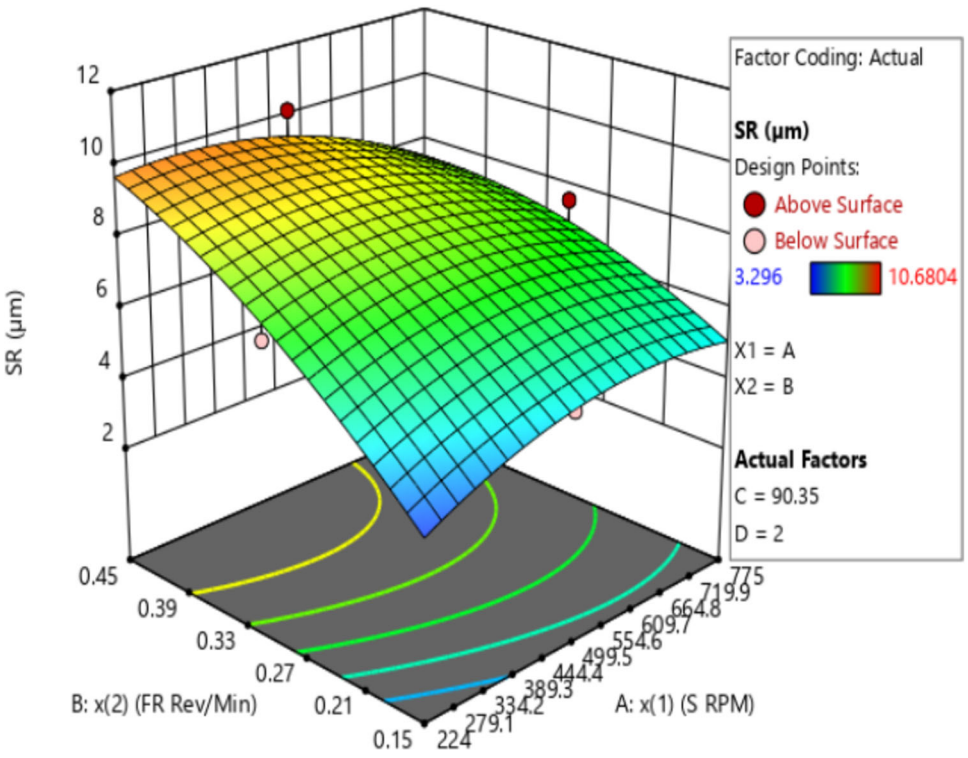

Fig. 15 SR effect on FR and Speed

Table 9 Influence of parameter's effect over MRR

Source	SS	DF	MS	F-value	p-value	
Model	8.125E + 06	14	5.803E + 05	14.19	< 0.0001	significant
A–x (1)	5.127E + 05	1	5.127E + 05	12.54	0.0041	significant
B-x (2)	1.494E + 05	1	1.494E + 05	3.65	0.0801	
C-x (3)	7.169E + 05	1	7.169E + 05	17.53	0.0013	significant
D-x (4)	2.600E + 06	1	2.600E + 06	63.57	< 0.0001	significant
AB	553.68	1	553.68	0.0135	0.9093	
AC	41,080.49	1	41,080.49	1.00	0.3360	
AD	28,575.84	1	28,575.84	0.6987	0.4196	
BC	28,317.03	1	28,317.03	0.6923	0.4216	
BD	1156.18	1	1156.18	0.0283	0.8693	
CD	74,801.78	1	74,801.78	1.83	0.2012	
A^2	607.13	1	607.13	0.0148	0.9050	
B^2	68,909.56	1	68,909.56	1.68	0.2187	
C^2	1.933E + 06	1	1.933E + 06	47.26	< 0.0001	significant
D^2	5.363E + 05	1	5.363E + 05	13.11	0.0035	significant
Lack of Fit	4.883E + 05	10	48,827.85	38.53	0.0256	
Pure Error	2534.28	2	1267.14			
Total	8.616E + 06	26				

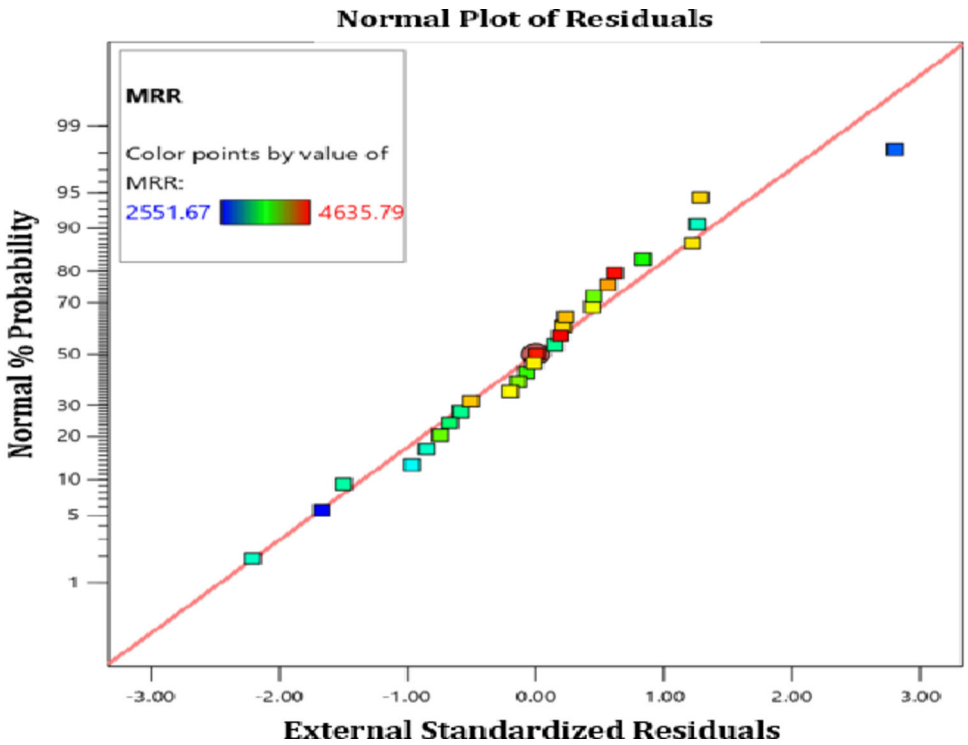

Fig. 16 Residuals plot for MR

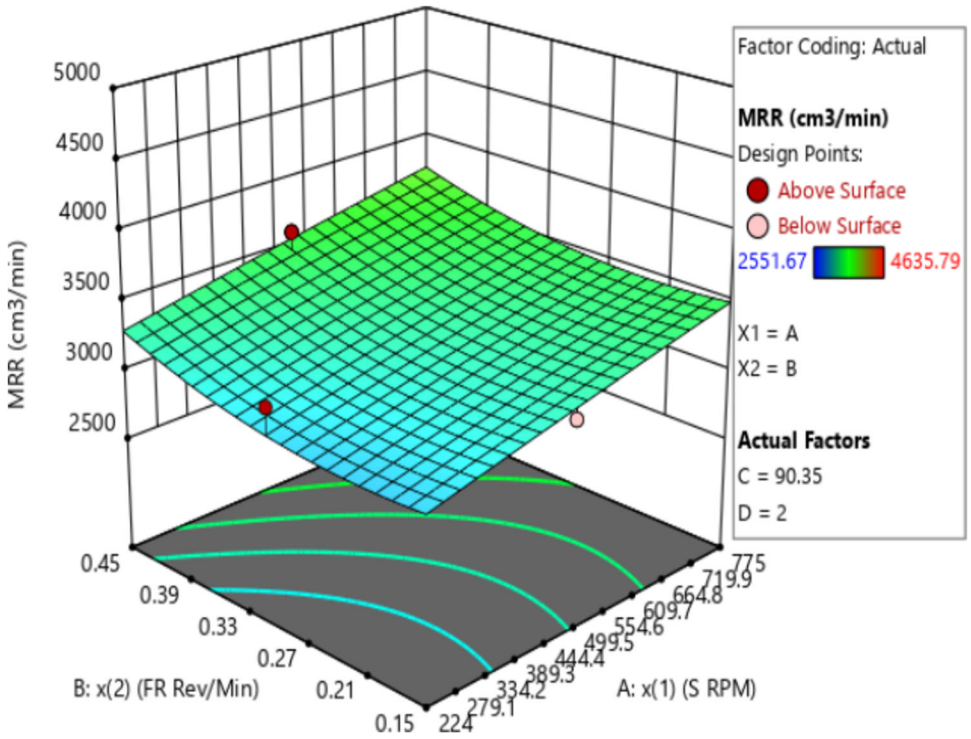

Fig. 17 MRR effect on FR and Speed

Table 10 Influence of parameter's effect over Insert tip Temperature

Source	SS	DF	MS	F-value	p-value	
Model	4580.39	14	327.17	8.95	0.0003	significant
A–x (1)	152.34	1	152.34	4.17	0.0638	
B-x (2)	1349.04	1	1349.04	36.91	< 0.0001	significant
C-x (3)	208.61	1	208.61	5.71	0.0342	significant
D-x (4)	319.94	1	319.94	8.75	0.0120	significant
AB	61.15	1	61.15	1.67	0.2202	
AC	83.01	1	83.01	2.27	0.1577	
AD	941.26	1	941.26	25.75	0.0003	significant
BC	4.17	1	4.17	0.1142	0.7413	
BD	79.83	1	79.83	2.18	0.1652	
CD	4.30	1	4.30	0.1176	0.7376	
A^2	539.98	1	539.98	14.77	0.0023	significant
B^2	14.82	1	14.82	0.4055	0.5362	
C^2	36.78	1	36.78	1.01	0.3356	
D^2	0.0710	1	0.0710	0.0019	0.9656	
Lack of Fit	322.41	10	32.24	0.5547	0.7855	
Pure Error	116.24	2	58.12			
Total	5019.04	26				

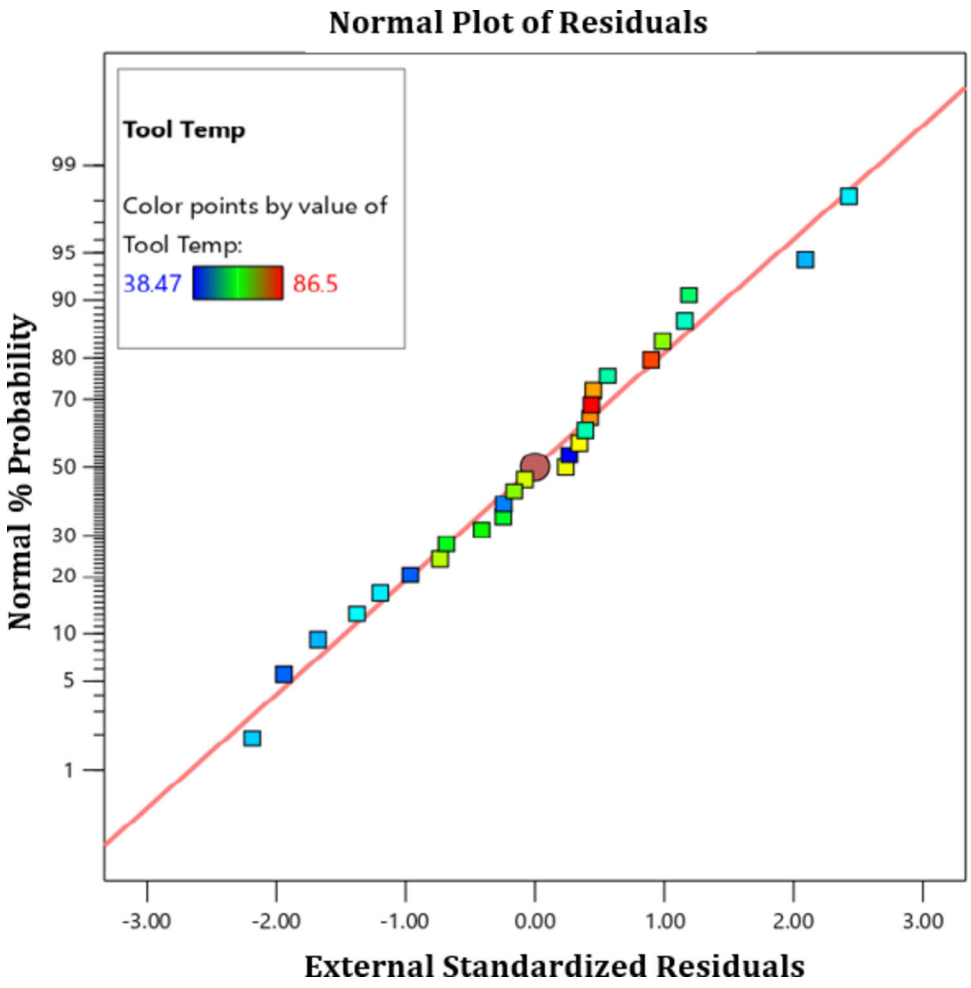

Fig. 18 Residuals plot for Tool tip temperature

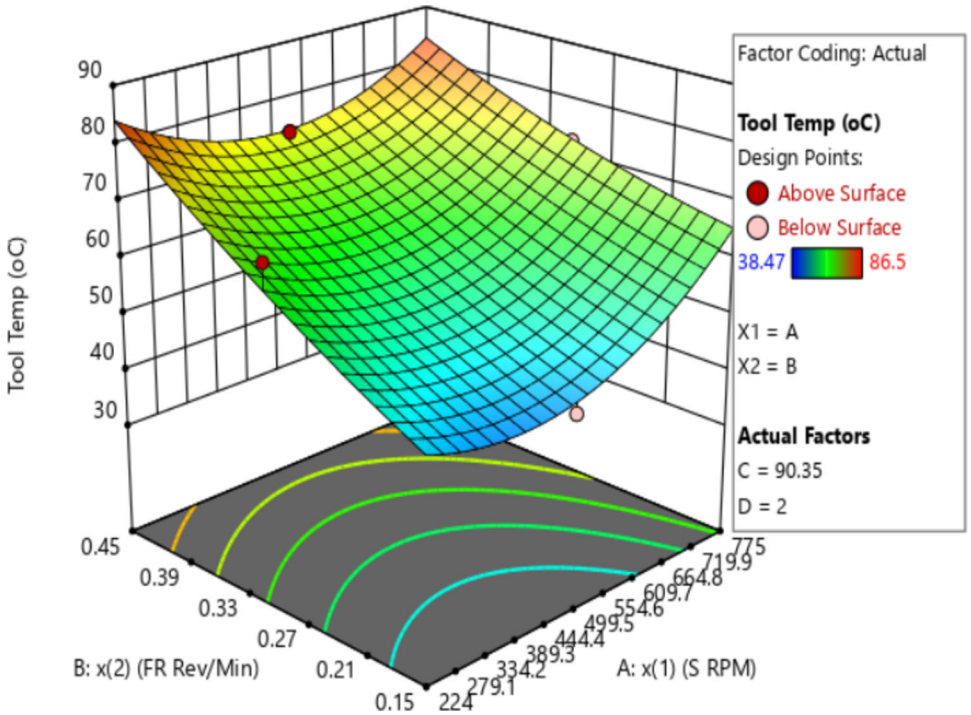

Fig. 19 Insert Tip Temperature effect on FR and Speed

Table 11 Influence of parameter's effect over Insert flank wear

Source	SS	DF	MS	F-value	p-value	
Model	0.2490	13	0.0192	10.07	< 0.0001	significant
A–x (1)	0.0000	1	0.0000	0.0054	0.9426	
B-x (2)	0.0118	1	0.0118	6.21	0.0270	significant
C-x (3)	0.0016	1	0.0016	0.8423	0.3755	
D-x (4)	0.0036	1	0.0036	1.92	0.1895	
AB	0.0014	1	0.0014	0.7322	0.4077	
AC	0.0057	1	0.0057	3.02	0.1060	
AD	0.0176	1	0.0176	9.28	0.0094	significant
BC	0.0003	1	0.0003	0.1418	0.7125	
BD	0.0121	1	0.0121	6.36	0.0255	significant
CD	0.0001	1	0.0001	0.0321	0.8607	
B^2	0.0088	1	0.0088	4.63	0.0507	significant
C^2	0.0632	1	0.0632	33.22	< 0.0001	significant
D^2	0.0723	1	0.0723	38.03	< 0.0001	significant
Lack of Fit	0.0247	11	0.0022	153.00	0.0065	
Pure Error	0.0000	2	0.0000			
Cor Total	0.2737	26				

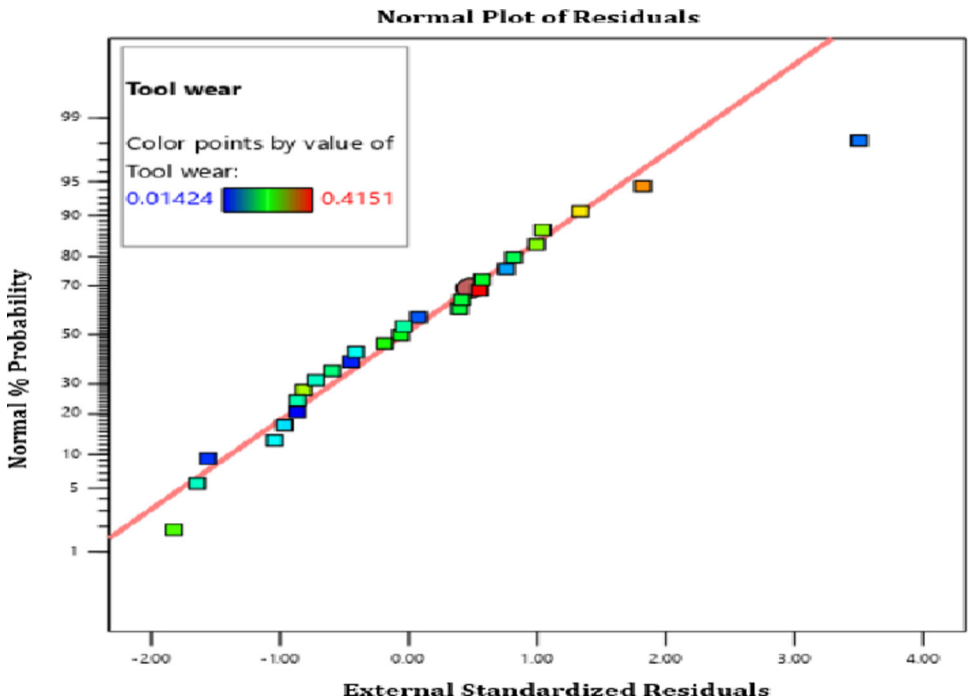

Fig. 20 Residuals plot for Insert wear

tabulated in Table 11. This method is applied to check the developed model's significance and the parameters effect over flank wear. In the P column, the lowest values indicate statistical significance for the response flank wear. In Fig. 20 the residuals of statistical analysis by ANOVA following the recorded values of response insert flank wear. The values of residuals are scattered around the zero-line indicating the model is adequate.

Figure 21 represents the relationship between insert flank wear and the parameters of the 3D surface plot. Providing the variation in flank wear values by varying the feed and speed. By increasing the feed rate the value of flank wear increased continuously at the lowest speed. The lowest flank wear is observed at 0.44 mm/rev feed and 224 rpm speed. This lowest value is recorded for M2 cast material and the NC-1 cooling environment.

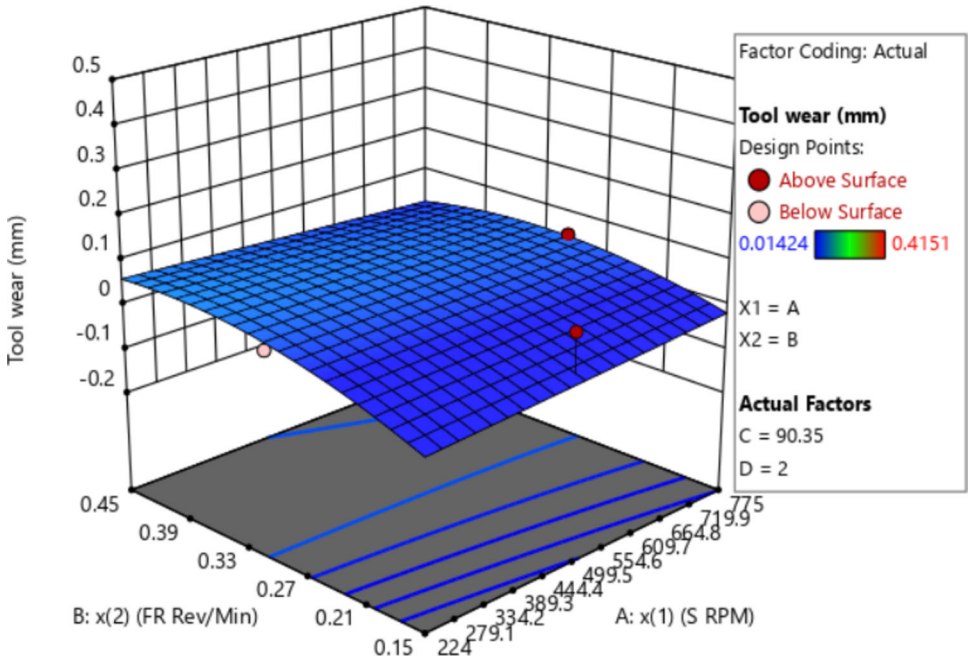

Fig. 21 Insert wear effect on FR and Speed

Table 12 Influence of parameter's effect over feed force

Source	SS	DF	MS	F-value	p-value	
Model	103.01	13	7.92	9.24	0.0001	significant
A–x (1)	0.0001	1	0.0001	0.0001	0.9923	
B-x (2)	36.66	1	36.66	42.74	< 0.0001	significant
C-x (3)	6.86	1	6.86	8.00	0.0142	significant
D-x (4)	21.80	1	21.80	25.41	0.0002	significant
AB	0.0069	1	0.0069	0.0081	0.9297	
AC	0.5714	1	0.5714	0.6661	0.4291	
AD	0.5625	1	0.5625	0.6557	0.4327	
BC	0.0159	1	0.0159	0.0185	0.8939	
BD	0.2500	1	0.2500	0.2914	0.5984	
CD	0.6451	1	0.6451	0.7520	0.4016	
B^2	0.4668	1	0.4668	0.5442	0.4738	
C^2	1.04	1	1.04	1.21	0.2906	
D^2	16.83	1	16.83	19.62	0.0007	significant
Lack of Fit	11.15	11	1.01			
Pure Error	0.0000	2	0.0000			
Cor Total	114.16	26				

6.2.5 Feed force analysis

The regression of RSM's feed force with speed, FR, hardness of cast composites, and cooling environment is tabulated in Table 12. In the research, the ANOVA analysis is done by design expert software considering a confidence level of 90 percent. In Fig. 22 the residuals of statistical analysis by ANOVA following the recorded values of response feed force. The values of residuals are scattered around the zero-line indicating the model is adequate. The values are very close to each other; hence, the model developed for feed force is significant.

Figure 23 represents the relationship between feed force and the parameters of the 3D surface plot. Providing the variation in feed force values by varying the feed and speed. By increasing the feed rate and speed the value of feed force increased continuously. The lowest feed force is observed at

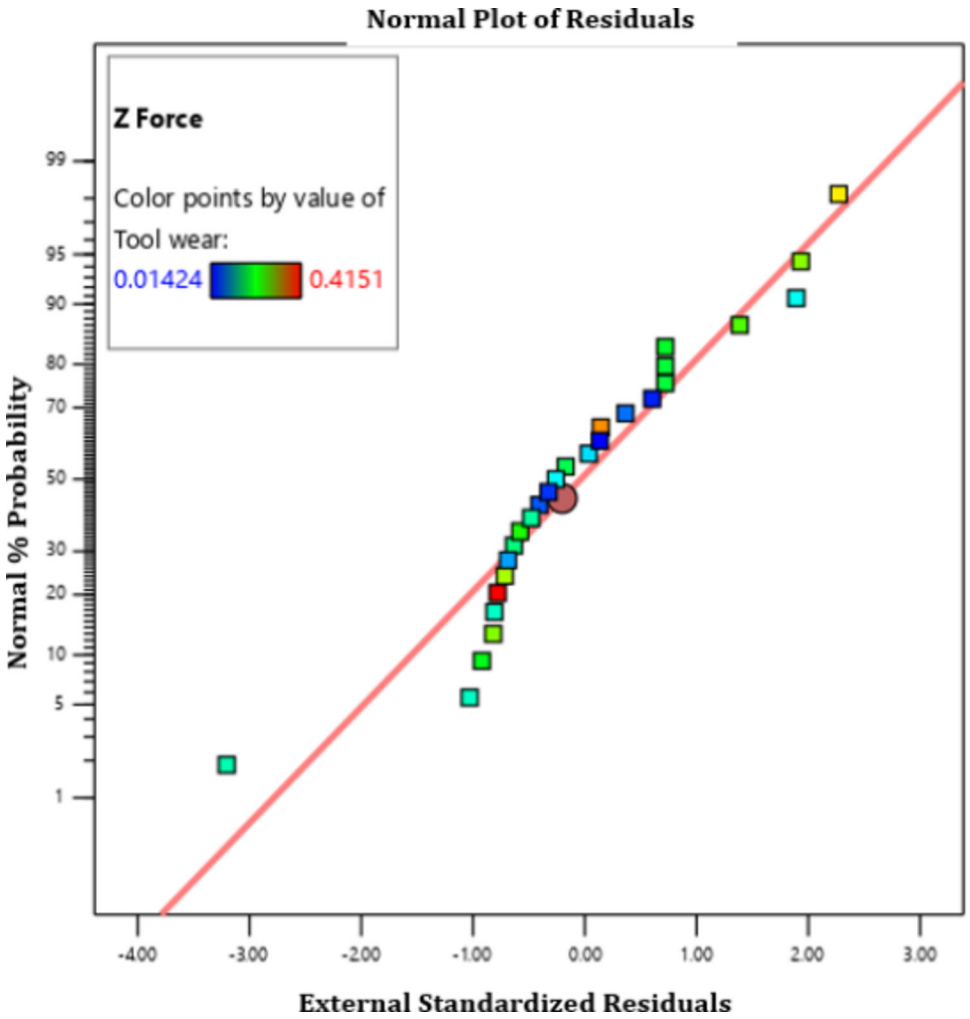

Fig. 22 Residual plot for Feed force

0.15 mm/rev feed and 224 rpm speed. This lowest value is recorded for M2 cast material and the NC-1 cooling environment.

6.3 Optimisation of responses by MOGA

The MOGA is applied for the responses to study the Pareto plots for MRR vs all other responses, the plots are represented in Fig. 24a, b, c, d. Equations 7 is represented by MRR, whereas the Eqs. 8, 9, 10 11 are SR, ITT, IFW, and ZFF respectively. The simultaneous prediction of lowest surface roughness at the same place the highest MRR is extracted in the graph Fig. 24 a. The SR of 2.4 μm at that point the 3574 mm^3/min MRR is observed. This result is at 224 rpm speed, 0.159 mm/rev feed, for M1 cast composite, and NC2 coolant. In comparison with experimental results roughness is improved by 0.86 μm. In Fig. 24 b the 32.59 °C lowest tip temperature is observed for that point and 3984 mm^3/min MRR is extracted. This is observed at 247.6 rpm speed, 0.159 mm/rev feed, for M3 cast composite, and NC2 coolant. In comparison with experimental results temperature is improved by 5.88 °C.

In Fig. 24 c the 0.0132 mm lowest insert flank wear is observed for that point and 2847 mm^3/min MRR is extracted. This is observed at 224 rpm speed, 0.18 mm/rev feed, for M1 cast composite, and NC1 coolant. Compared to test results 0.001 mm is improved. In Fig. 24 d the 1.25 kgf lowest feed force is observed for that point 4248 mm^3/min MRR is extracted. This is observed at 247.6 rpm speed, 0.159 mm/rev feed, for M1 cast composite, and NC2 coolant. The feed force is 0.25 kgf more than the experimental results.

6.4 Optimisation of responses by MOPSO

The MOPSO is applied for the responses to study the Pareto plots for MRR vs all other responses, the plots are represented in Fig. 25. a, b, c, d. The simultaneous prediction of lowest surface roughness at the same place the highest MRR is extracted in the graph Fig. 25 a. The SR of 3.5 μm at that point the 3059 mm^3/min MRR is observed. This result is at

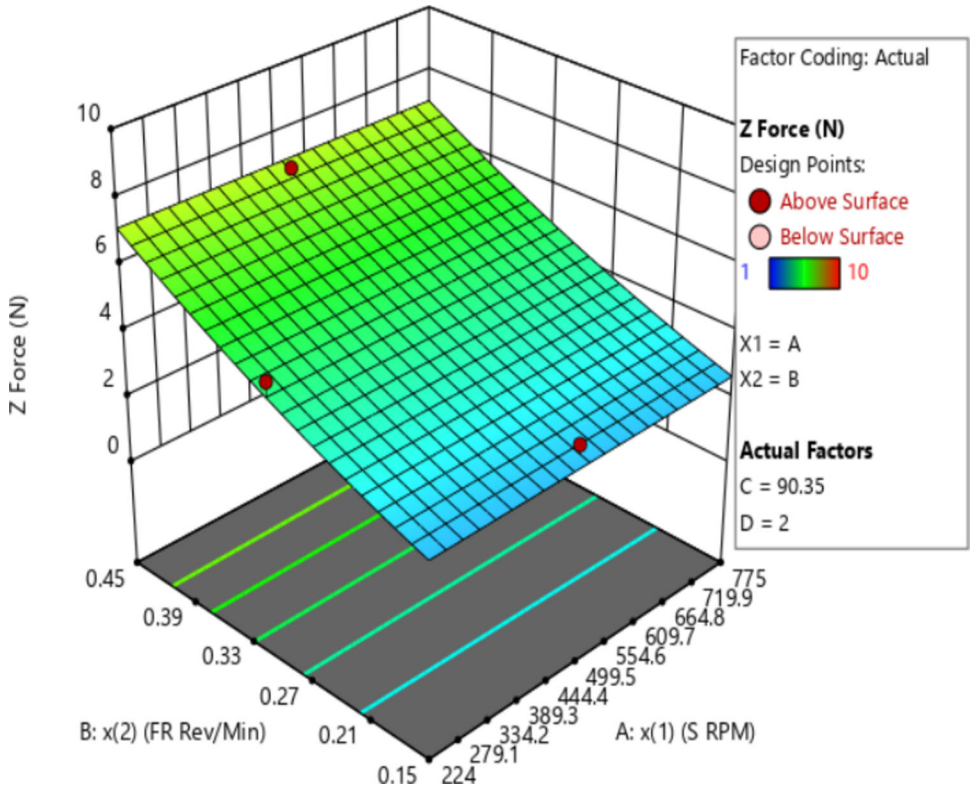

Fig. 23 Feed force effect on FR and Speed

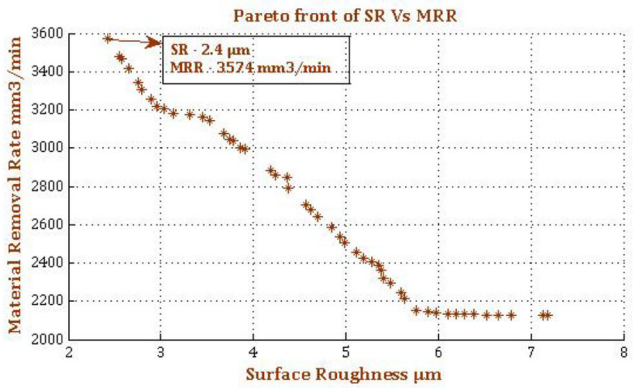

a. Pareto plot for SR vs MRR

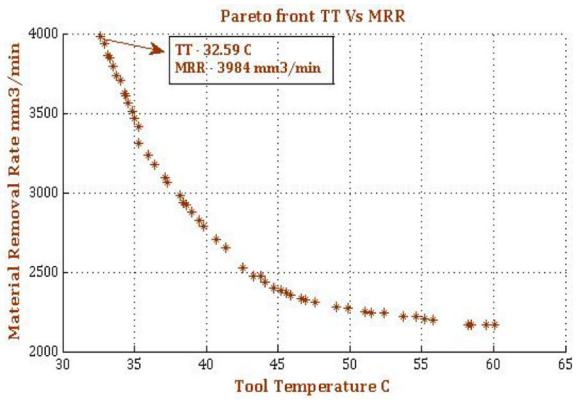

b. Pareto plot for ITT vs MRR

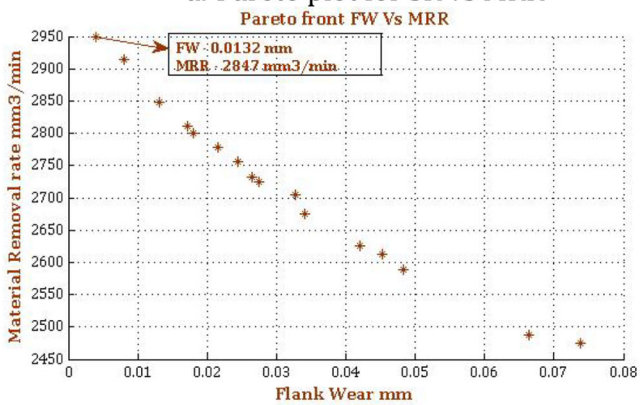

c. Pareto plot for IFW vs MRR

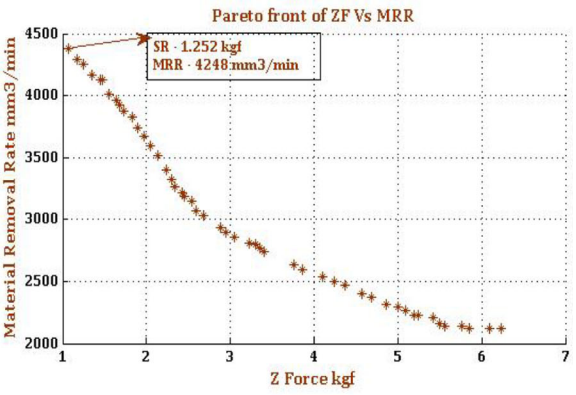

d. Pareto plot for FF vs MRR

Fig. 24 MOGA generated pareto plots for MRR Vs Responses

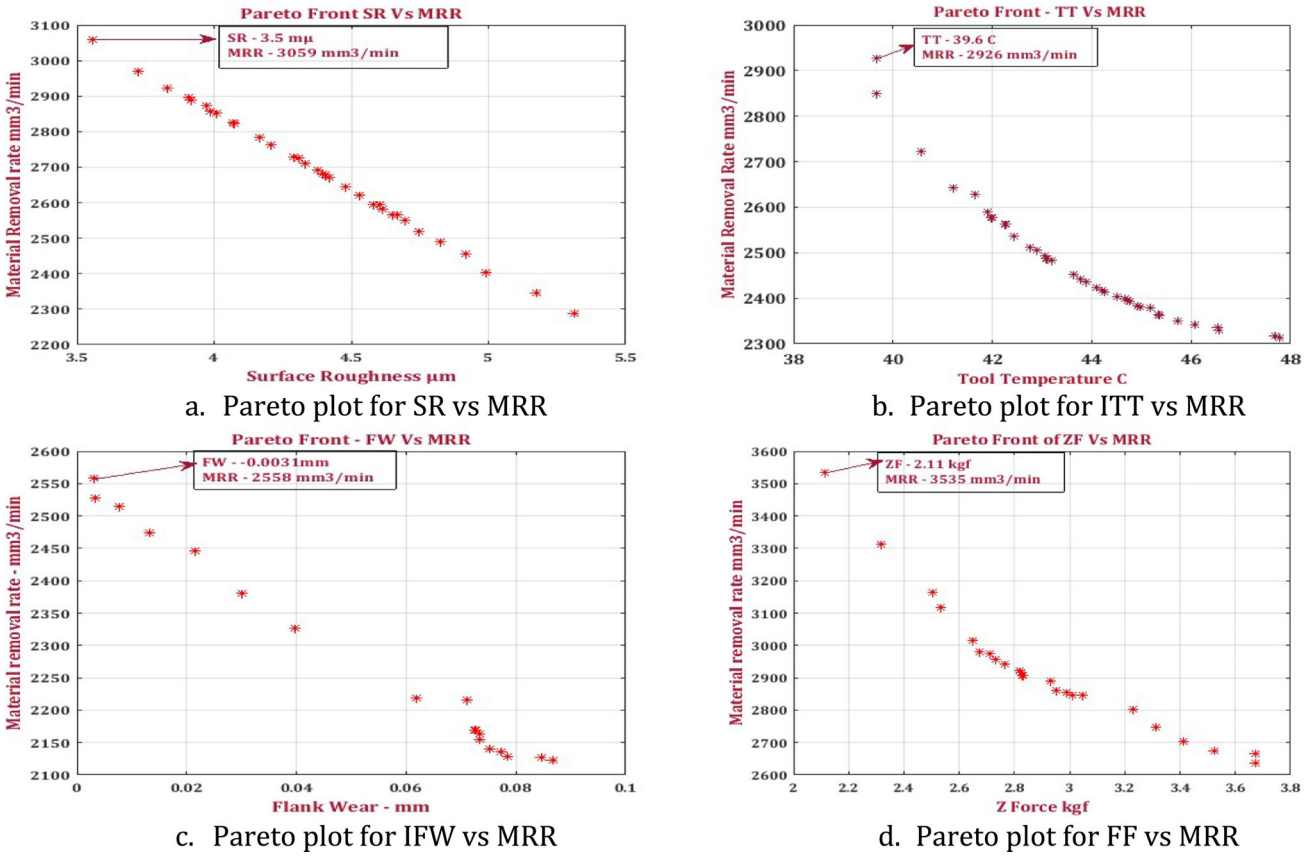

Fig. 25 MOPSO generated pareto plots for MRR Vs Responses

224 rpm speed, 0.159 mm/rev feed, for M1 cast composite, and NC1 coolant. In comparison with experimental results, roughness is lagging by 0.3 μm. In Fig. 25 b the 39.6 °C lowest tip temperature is observed for that point and 2926 mm^3/min MRR is extracted. This is observed at 560.9 rpm speed, 0.159 mm/rev feed, for M3 cast composite, and NC2 coolant. In comparison with experimental results temperature is lagging by 1.13 °C.

In Fig. 25 c the 0.0032 mm lowest insert flank wear is observed for that point and 2558 mm^3/min MRR is extracted. This is observed at 224 rpm speed, 0.159 mm/rev feed, for M2 cast composite, and NC1 coolant. In Fig. 25 d the 2.1 kgf lowest feed force is observed for that point and 3535 mm^3/min MRR is extracted. This is observed at 385 rpm speed, 0.159 mm/rev feed, for M3 cast composite, and NC2 coolant. The feed force is 1.1 kgf more than the experimental results.

6.5 Optimisation of responses by MONSG 2

The MONSG 2 is applied for the responses to study the Pareto plots for MRR vs all other responses, the plots are represented in Fig. 26a, b, c, d. The simultaneous prediction of lowest surface roughness at the same place the highest MRR is extracted in the graph Fig. 26 a. The SR of 3.0 μm at that point the 3339 mm^3/min MRR is observed. This result is at 237 rpm speed, 0.159 mm/rev feed, for M1 cast composite, and NC2 coolant. In comparison with experimental results roughness is improved by 0.2 μm. In Fig. 26 b the 33.68 °C lowest tip temperature is observed for that point 3688 mm^3/min MRR is extracted. This is observed at 242.8 rpm speed, 0.159 mm/rev feed, for M3 cast composite, and NC2 coolant. In comparison with experimental results temperature is improved by 4.79 °C. In Fig. 26 c the 0.0184 mm lowest insert flank wear is observed for that point 2534 mm^3/min MRR is extracted. This is observed at 265 rpm speed, 0.18 mm/rev feed, for M2 cast composite, and NC1 coolant. In Fig. 26 d the 1.41 kgf lowest feed force is observed for that point 4145 mm^3/min MRR is extracted. This is observed at 477 rpm speed, 0.159 mm/rev feed, for M3 cast composite, and NC1 coolant. The feed force is 0.41 kgf more than the experimental results.

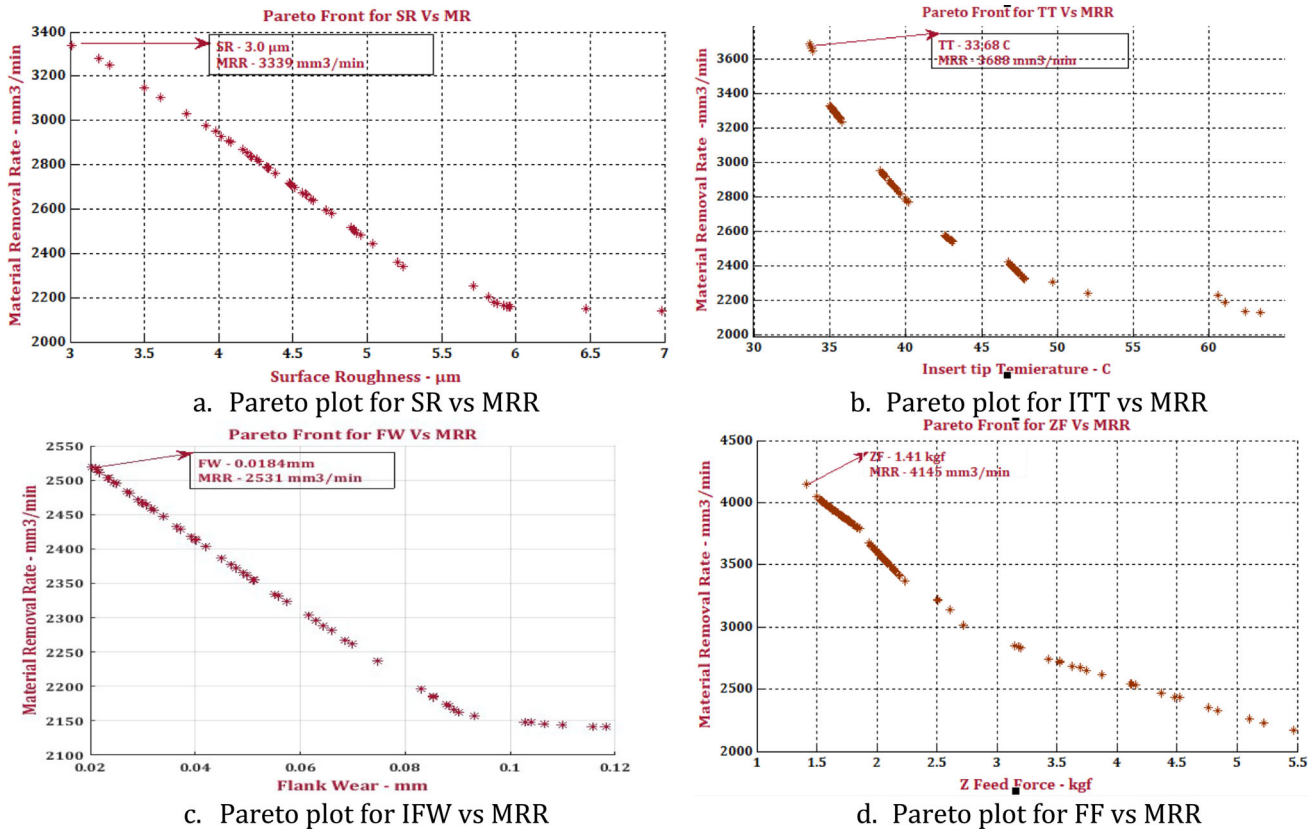

Fig. 26 MONSG2 generated pareto plots for MRR Vs Responses

Table 13 Percentage error between observed and predicted

Exp No	SR			MRR			ITT			IFW			ZFF		
	Exp	Pre	Error %	Exp	Pre	Error %	Exp	Pre	Error %	Exp	Pre	Error %	Exp	Pre	Error %
5	9.28	9.18	1.07	3184.72	3287.08	−3.21	68.76	69.36	− 0.87	0.2056	0.2074	− 0.87	5.75	6.28	− 9.21
11	6.53	6.04	7.50	3308.01	3379.33	−2.15	60.8	61.71	− 1.49	0.1666	0.1831	− 9.90	4.04	4.41	− 9.15
17	7.2	7.4	− 2.77	3377.5	3459.03	−2.41	46.9	40.34	13.98	0.4151	0.3998	3.68	6	6.45	− 7.5
22	8.97	9.02	− 0.55	4583.75	4582.7	0.02	79.8	78.23	1.96	0.3592	0.3156	12.13	6	5.92	1.33
24	7.6	6.98	8.15	3267.71	3497.13	−7.02	72.48	72.87	− 0.538	0.0493	0.0465	5.67	4.21	4.53	− 7.60

7 Validation for the experimental results

Table 13 represents the confirmation between experimental data and predicted data through RSM for all the models generated. The test numbers are randomly picked from Table 5 and the error percentage is evaluated by Eq. 12 [39]. The percentage error is less than ten percentage for SR, MRR, and feed force which indicates the models developed are optimal.

$$\text{percentage Error} = \frac{ER - PR}{ER} \times 100 \tag{12}$$

PR- Predicted results, ER- Experimental Results.

8 Data comparisons

In DFA analysis, at 775 rpm speed, 0.2995 mm/rev feed rate, Al_2O_3 coated inserts and NC 2 coolant are effective parameters to extract the best responses. The cast material M2 exhibits the required optimal settings in the study. From Fig. 10 the optimal factors are represented by S3FR2CH2CE3 and the responses recorded for the same are 6.391 µm roughness, 4609.55 mm3/min MRR, 86.5 insert temperature, 0.2255 mm insert flank wear (V_b), and 2.8 kgf force. In Fig, 11, 13, 15, 17, 19 the experimental and predicated value plots are shown graphically for SR, MRR, ITT, IFW, and ZFF respectively. The R^2 values of SR, MRR, ITT, IFW, and ZFF generated by RSM regression

are 0.9619, 0.9430, 0.9126, 0.9097, and 0.9023 respectively which are adequate. In all five residuals plot, the squared dots are indicating experimental data in which they are very closely aligned with the red residual line. In Fig, 12, 14, 16, 18, and 20 represent the relations between parameters and responses of the generated models. The generated models are utilized to study the effect of speed and feed rate with responses.

The MOGA, MOPSO, and MONSG2 optimisation methods generated Figs. 21, 22, 23, a to d represent the Pareto plot of response MRR versus other responses SR, ITT, IFW, FF. The plots of Pareto indicating the closeness of generated value with recorded value. Among three MATLAB techniques the lowest SR of 2.4 μm is generated by MOGA at 224 rpm speed, 0.159 mm/rev feed, for M1 cast composite and NC2 coolant. The 32.59 °C lowest tip temperature is observed at 247.6 rpm speed, 0.159 mm/rev feed, for M3 cast composite and NC2 coolant by MOGA. The lowest 0.0032 mm insert flank wear is observed at 224 rpm speed and 0.159 mm/rev feed for M2 cast composite and NC1 coolant by MOPSO. The lowest 1.25 kgf feed force is observed at 247.6 rpm speed, 0.159 mm/rev feed, for M1 cast composite, and NC2 coolant by MOGA. The MOGA dominates in generating better results compared to other techniques.

9 Conclusion

The research focused on the development of LM 25 cast composites in three different combinations, the nano TiO_2, nano ZrO_2, and fixed quantity of bagasse ash are used for all cast composite. The mechanical properties are studied for the prepared composite. The soyabean-based nano coolant is prepared by using $nTiO_2$, $nMOS_2$, and nZnO and used in the turning process in MAC condition. The uncoated and PVD-coated TiCN, Al_2O_3-coated carbide inserts are used in turning operations. The surface roughness, MRR, insert tip temperature, insert flank wear (V_b), and feed force are studied as responses. The RSM- BBD design is used to obtain test combinations, and to generate the fit models. The DFA is used for parameters optimisation. The MOGA, MOPSO, and MONSG2 MATLAB algorithms are used as soft optimisation techniques.

The conclusion of the research is:

- Prepared three composites providing improvement in mechanical properties compared to a base alloy. The LM 25 84% + 5% $nTiO_2$ + 3% $nZrO_2$ + 8% bagasse ash combination of reinforcement exhibits 96.20 HV microhardness with an improvement in hardness by 38.76 HV compared to the base alloy. The percentage increase in the hardness value improves the machining capabilities.
- The above combination of reinforcement exhibits 148 MPa tensile strength with an improvement of 18 MPa tensile strength compared to the base alloy. The fracture risk of material can be improved due to an increase in tensile strength of LM 25 Cast composite.
- The compression strength is 539.1 MPa with an improvement of 325.5 MPa. The improvement in compressive strength withstands the deformation of LM 25 Cast composite.
- The two different coating combinations are utilised in the research, from which the TiCN-coated inserts exhibit reduced tool wear compared to other coated and uncoated inserts. This coating of inserts helps in reduction of the temperature at contact zone.
- In the research the soybean cooking oil is used as a base oil to prepare nano coolant. The 1 wt % $nTiO_2$, 1.5 wt % $nMoS_2$ concentrations with soybean oil performed well by reducing roughness and insert flank wear. The use of this nano coolant, minimizes the friction at the contact zone and dissipates heat at a faster rate. The surface roughness, tool wear, and temperature will be reduced with an increase in the volume of material removal in the cutting process.
- The regression equations developed by RSM-BBD for all the responses show the significant characteristics. Providing adequate correlation between responses and parameters. The R^2 values of all responses are 0.9619, 0.9430, 0.9126, 0.9097, and 0.9023, which leads to adequate results. The developed regression models exhibit significant results.
- The optimal settings obtained from DFA are S3FR2CH2CE3, which is the highest speed 775-rpm, medium feed 0.299 mm/rev, M2 cast composite, with three nano particle concentration coolants. The responses are 6.391 μm roughness, 4609.55 mm3/min MRR, 86.5 insert temperature, 0.2255 mm insert flank wear (V_b), and 2.8 kgf force. These optimal settings lead to better responses.
- The soft computing optimisation methods like MOGA, MOPSO, and MONSG2 are applied to investigate the responses. The higher the better MRR versus all four lower the better SR, FW, ITT, and ZF responses are studied through the Pareto front plot. Among three MATLAB techniques the lowest SR of 2.4 μm is generated by MOGA at 224 rpm speed, 0.159 mm/rev feed, for M1 cast composite and NC2 coolant.
- The 32.59 °C lowest tip temperature is observed at 247.6 rpm speed, 0.159 mm/rev feed for M3 cast composite and NC2 coolant by MOGA. The MOGA generates best parametric combinations to reduce insert tip temperature.
- The lowest 0.0032 mm insert flank wear is observed at 224 rpm speed and 0.159 mm/rev feed for M2 cast composite and NC1 coolant by MOPSO. The MOPSO provides

best combination of input factors for lesser insert wear with long insert life. The lowest 1.25 kgf feed force is observed at 247.6 rpm speed, 0.159 mm/rev feed, for M1 cast composite, and NC2 coolant by MOGA. The MOGA dominates in generating better parameters for cutting force compared to other techniques.

10 Future scope

The LM 25 cast composites developed in this research are widely used in the sectors where the lightweight, corrosion-resistant cast composites are already common like, marine, automotive parts, and aerospace. The promising mechanical properties are obtained from the reinforcements of a combination of nano TiO_2, nano ZrO_2, and bagasse ash with LM 25. The better improvement in hardness, tensile and compression strength leads to the production of components like clutches, brake, valve bodies, and suspension brackets, where hardness and compressive strength are required.

The variation of base material LM25, selected nano material and variation in bagasse ash can be developed to study the mechanical properties, wear and other related properties to meet the industrial applications. The different nano materials with base material can also be developed for the future study to check the improvement in material properties. Further work can extend the machining studies to high-speed CNC environments, different tool geometries and coatings, and real production cycles to validate tool-life and energy-saving benefits under factory conditions. The different techniques are utilized to optimise accurately the input parameters for the industrial need.

Acknowledgements Shree. M. R. Halagond, instructor. Shree. Satish Mendegar, Technicians. Shree. C. M. Math. Technicians

Author Contributions All the authors have contributed equally**.**

Funding No funding.

Declarations

Competing of interest The author declares that No Competing of interest.

Consent to participate As the article does not involve any biological aspects thus "Consent to participate" does not apply.

References

1. Ramasubbu, N., Kulandaivel, D., Raj, J.A.: Influence of different squeeze pressures on metallurgical and tribological behavior of A356 silicon carbide and MoS2-based hybrid composites. J. Inst. Eng. India Ser. D (2024). https://doi.org/10.1007/s40033-024-00763-z
2. Prakash, C., Senthil, P., Manikandan, N., Palanisamy, D.: Investigations and regression modeling on mechanical characterization of cast aluminum alloy based (LM 26+ graphite+ fly ash) hybrid metal matrix composites. Int. J. Interact. Des. Manufact. (2022). https://doi.org/10.1007/s12008-022-00881-6
3. Rajendar, K., Eswaraiah, K.: Experimental investigation and optimization for friction and wear behavior of aluminum LM 25/h-BN/B4C composites via mixture design and desirability approach. Int. J. Interact. Des. Manufact. **18**(4), 2017–2029 (2024). https://doi.org/10.1007/s12008-022-00931-z
4. Anusha, P., Sri, M.N.S., Vijayakumar, S., Rao, T.J., Paramasivam, P., Jeyakrishnan, S., Saxena, K.K.: Design and optimization the wear characteristics for Al7178/TiO2/B4C/FA central hybrid composite. Int. J. Interact. Des. Manufact. **18**(8), 5773–5781 (2024). https://doi.org/10.1007/s12008-023-01341-5
5. Prathap Singh, S., Suresh Kumar, S., Elil Raja, D., Sonar, T., Ivanov, M., Velmurugan, G., Perumal, A.: Machinability studies on AA–SiC–TIO2 based heat treated HMMC with negative polarity electrode using EDM. Int. J. Interact. Des. Manufact. **18**(7), 5165–5176 (2024). https://doi.org/10.1007/s12008-023-01605-0
6. Radhika, N., Sai Charan, K.: Experimental analysis on three body abrasive wear behaviour of stir cast Al LM 25/TiC metal matrix composite. Trans. Indian Inst. Met. **70**, 2233–2240 (2017). https://doi.org/10.1007/s12666-017-1061-6
7. Sarvani, R.K., Mohinoddin, M., Ramakrishna, L.S.: Characterization and mechanical testing of hybrid metal composites of aluminium alloy (A356/LM25) reinforced by micro-sized ceramic particles. J. Inst. Eng. India Ser. C **105**(3), 457–470 (2024). https://doi.org/10.1007/s40032-024-01064-w
8. Kumara, B., Preetham Kumar, G.V.: Investigation on microstructure and mechanical properties of solution heat-treated and multi directional forging-processed LM-25 aluminium alloy. Trans. Indian Inst. Met. **73**(6), 1561–1566 (2020). https://doi.org/10.1007/s12666-020-01924-w
9. Singh, S.P., Raja, D.E., Ananthapadmanaban, D., Sonar, T., Ivanov, M.: Analyzing the effect of WEDM parameters on machining of heat treated SiC and TiO2 reinforced LM25 aluminium alloy hybrid composite using Taguchi methodology. Int. J. Interact. Des. Manufact. **19**(1), 37–46 (2025). https://doi.org/10.1007/s12008-023-01417-2
10. Ponnusamy, P., Tamil peruvalathan, S.: Performance evaluation and hybrid deep recurrent neural network-based prediction of SS304 turning characteristics using nanoparticles added water emulsified MQL. Biomass Conv. Bioref. **13**(8), 7349–7373 (2023)
11. Tiwari, S., Amarnath, M., Gupta, M.K.: Synthesis, characterization, and application of Al2O3/coconut oil-based nanofluids in sustainable machining of AISI 1040 steel. J. Mol. Liq. **386**, 122465 (2023). https://doi.org/10.1016/j.molliq.2023.122465
12. Tiwari, S., Amarnath, M., Gupta, M.K., Makhesana, M.A.: Performance assessment of nano-Al2O3 enriched coconut oil as a cutting fluid in MQL-assisted machining of AISI-1040 steel. Int. J. Adv. Manuf. Technol. **129**(3), 1689–1702 (2023). https://doi.org/10.1007/s00170-023-12394-x
13. Faheem, A., Husain, T., Hasan, F., Murtaza, Q.: Effect of nanoparticles in cutting fluid for structural machining of Inconel 718. Adv. Mater. Process. (2020). https://doi.org/10.1080/2374068x
14. Tuan, N.M., Duc, T.M., Long, T.T., Hoang, V.L., Ngoc, T.B.: Investigation of machining performance of MQL and MQCL hard turning using nano cutting fluids. Fluids **7**(5), 143 (2022). https://doi.org/10.3390/fluids7050143
15. Eltaggaz, A., Nouzil, I., Deiab, I.: Machining Ti-6Al-4V alloy using nano-cutting fluids: investigation and analysis. J. Manuf. Mater. Process. **5**(2), 42 (2021). https://doi.org/10.3390/jmmp5020042

16. Dash, L., Padhan, S., Das, S.R.: Experimental investigations on surface integrity and chip morphology in hard tuning of AISI D3 steel under sustainable nanofluid-based minimum quantity lubrication. J. Braz. Soc. Mech. Sci. Eng. **42**(10), 500 (2020). https://doi.org/10.1007/s40430-020-02594-x
17. St, P.K., Hp, T.P., Siddaraju, C.: Investigate the effect of Al2O3 and CuO nano cutting fluids under MQL technique in turning of DSS-2205. Adv. Mater. Process. Technol. **8**(3), 3297–3330 (2022). https://doi.org/10.1080/2374068X.2021.1948701
18. Hamdi, A., Yapan, Y.F., Uysal, A., Merghache, S.M.: Machinability assessment and optimization of turning AISI H11 steel under various minimum quantity lubrication (MQL) conditions using nanofluids. Int. J. Adv. Manuf. Technol. (2025). https://doi.org/10.1007/s00170-025-15418-w
19. Buldum, B.B., Leksycki, K., Cagan, S.C.: Comparative analysis of dry, minimum quantity lubrication, and nano-reinforced minimum quantity lubrication environments on the machining performance of AZ91D Magnesium Alloy. Machines **13**(5), 430 (2025). https://doi.org/10.3390/machines13050430
20. Efa, D.A., Dejene, N.D., Ifa, D.A., Nemomsa, S.K., Gemechu, T.B.: Improving computer numerical control (CNC) turning performance of AISI D2 steel with nanofluid composites and advanced machine learning techniques. Int. J. Adv. Manuf. Technol. (2025). https://doi.org/10.1007/s00170-025-15536-5
21. Bhowmik, A., Kumar, R., Jhala, R., Beemkumar, N., Kumar, A.V., Kedia, A., Kumar, K.D.H., Singh, G.: Advanced machining of inconel 690 using alumina-enriched sunflower oil-based lubricant: a genetic algorithm-driven approach. Int. J. Interact. Des. Manuf. (2025). https://doi.org/10.1007/s12008-025-02246-1
22. Kuntoğlu, M., Binali, R., Makhesana, M.: Characterizing machining indicators with machine learning models under cellulose nanocrystal and graphene-based nanofluid conditions. Arabian J. Sci. Eng. (2025). https://doi.org/10.1007/s13369-025-10240-8
23. Raut, L.P., Vinchurkar, S.M., Kalbande, V.P., Choudhari, M.S., Purohit, N., Tawele, P., Awate, N.: Impact of Al2O3 nanofluid on vibration and temperature reduction in machining. Iran. J. Sci. Technol. Trans. Mech. Eng. (2025). https://doi.org/10.1007/s40997-025-00880-4
24. Ali, A.R.I., Salam, B.: A review on nanofluid: preparation, stability, thermophysical properties, heat transfer characteristics and application. SN Appl. Sci. **2**(10), 1636 (2020). https://doi.org/10.1007/s42452-020-03427-1
25. Ross, N.S., Ganesh, M., Ananth, M.B.J., Kumar, M., Rai, R., Gupta, M.K., Korkmaz, M.E.: Development and potential use of MWCNT suspended in vegetable oil as a cutting fluid in machining of Monel 400. J. Mol. Liq. **382**, 121853 (2023). https://doi.org/10.1016/j.molliq.2023.121853
26. Sharma, S., Das, P.P., Ladakhi, T.Y., Pradhan, B.B., Phipon, R.: Comparative assessment of machining efficiency in turning of Ti-6Al-4V alloy under dry, wet, and MQL conditions. Int. J. Interact. Des. Manuf. (2024). https://doi.org/10.1007/s12008-024-02181-7
27. Sankaranarayanan, R., Krolczyk, G.M.: A comprehensive review on research developments of vegetable-oil based cutting fluids for sustainable machining challenges. J. Manuf. Process. **67**, 286–313 (2021). https://doi.org/10.1016/j.jmapro.2021.05.002
28. Wang, W., Lin, H., Zhou, M., Xie, H., Dai, B., Han, S.: Formulation, characterization, mechanism, and application of vegetable oil-based nano-cutting fluids. Int. J. Adv. Manuf. Technol. (2025). https://doi.org/10.1007/s00170-024-14973-y
29. Volke, P., Saelzer, J., Zabel, A., Biermann, D.: Influence of cutting tool coating on rake and flank face temperatures by operando pyrometric temperature measurement during orthogonal turning of AISI 316L. Wear (2025). https://doi.org/10.1016/j.wear.2025.205848
30. Sirtuli, L.J., Boing, D., Bushlya, V., Norgren, S.: Study of initial notch wear during turning of stainless steel with (CVD) Al2O3/Ti(C, N) coated cemented carbide tools. Int. J. Refract. Met. Hard Mater. (2025). https://doi.org/10.1016/j.ijrmhm.2025.107116
31. Sen, B., Saha, S., Kumar, R., Jhala, R., Patil, N., Mahapatro, A., Bhowmik, A.: AI-driven wear monitoring of PVD TiAlN coated carbide insert in sustainable machining of Hastelloy C276: an industry 4.0 perspective. Results Eng. **25**, 104457 (2025). https://doi.org/10.1016/j.rineng.2025.104457
32. Barik, E.S., Jena, P.C., Behera, R.K., Sethy, S., Das, S.R.: Experimental investigation and sustainability assessment in turning of newly developed AMMC (Al–Mg–Si–Cu–SiC) using coated carbide tool under minimum quantity lubrication. Arab. J. Sci. Eng. (2025). https://doi.org/10.1007/s13369-024-09957-9
33. Zhao, J., Liu, Z.: Influences of coating thickness on cutting temperature for dry hard turning Inconel 718 with PVD TiAlN coated carbide tools in initial tool wear stage. J. Manuf. Process. **56**, 1155–1165 (2020). https://doi.org/10.1016/j.jmapro.2020.06.010
34. Gao, L., Liu, C., Hou, Z., Li, C., Shen, R., Yang, T.: Dry turning of SiCp/Al matrix composites with a wide range of particle volume fractions: tool wear characteristics analysis of multi-coated tool. Int. J. Adv. Manuf. Technol. **121**(7), 5343–5359 (2022). https://doi.org/10.1007/s00170-022-09727-7
35. Fernandes, G.H.N., Barbosa, L.M.Q., França, P.H.P., Martins, P.S., Machado, Á.R.: Towards green manufacturing: investigating tool coatings and cooling strategies for Inconel 718 turning. Int. J. Adv. Manuf. Technol. **129**(5), 2257–2279 (2023). https://doi.org/10.1007/s00170-023-12390-1
36. Syed, H.S., De Paiva, J.M., Veldhuis, S.C.: Wear and micromechanical performance of novel mono/bi-layered PVD-coated WC tools in high-speed turning of Ti-5Al-5V-5Mo-3Cr alloy. Int. J. Adv. Manuf. Technol. **133**(9), 4939–4955 (2024). https://doi.org/10.1007/s00170-024-14045-1
37. Amin, A.K.M., Khatun, S., Saba, T., Iqbal, M., Rumi, M.J.U.: High-speed machining of INCONEL 718: enhancing surface roughness and tool life using TiN-coated carbide tools. Int. J. Adv. Manuf. Technol. **138**(5), 1965–1994 (2025). https://doi.org/10.1007/s00170-025-15558-z
38. Liu, X., Li, Y., Zhang, X., Cheng, X., Mu, L., Gao, C., Zhang, Z.: FE study on the effect of heat transfer on cutting temperature and cutting force in heat-assisted cutting of superalloy Inconel 718 using coated tools. Int. J. Adv. Manuf. Technol. (2025). https://doi.org/10.1007/s00170-025-15817-z
39. Muniyappan, K., Guttula, R., Dhapekar, N.K., N, L., Singh, R., Pathak, V.K.: Optimization of cutting force during turning of custom 450 steel using TiAlSiN coated WC tool inserts. Int. J. Interact. Des. Manuf. **19**(4), 2865–2882 (2025). https://doi.org/10.1007/s12008-024-01934-8
40. Shafeeque, T., George, A., Mathew, J., Kuriachen, B.: Force modeling and experimental investigations on machinability of SDSS 2507 under dry turning conditions using CVD TiCN-Al2O3 coated tools. Sādhanā **49**(3), 236 (2024). https://doi.org/10.1007/s12046-024-02585-x
41. Das, A., Kumar, A., Padhan, S., Das, S.R., Satpathy, M.P., Patel, S.K.: Hard turning of AISI H10 steel using AlTiN and AlTiSiN coated carbide tools: comparative machining performance evaluation and economic assessment. J. Braz. Soc. Mech. Sci. Eng. **46**(5), 277 (2024). https://doi.org/10.1007/s40430-024-04855-5
42. Patnaik, L., Kumar, S., Gajjar, J., Dash, P., Maity, S.R., Łępicka, M., Devi, P.B.: Box-behnken based investigation of surface quality and tool wear rate and FEM analysis of tool wear in TiAlN/CrN coated carbide tool. Int. J. Interact. Des. Manufact. **18**(9), 6381–6396 (2024). https://doi.org/10.1007/s12008-022-01146-y
43. Praveen, N., Ng, S.K., Prasad, C.D., Soni, H., Prasad, M., Tc, S.K., Mallik, U.S., Aden, A.A.: Effect of CNC turning parameters on MRR, cutting force and surface roughness for ternary shape memory alloys (SMAs). Results Eng. **26**, 104876 (2025). https://doi.org/10.1016/j.rineng.2025.104876

44. Amigo, F.J., Urbikain, G., de Lacalle, L.L., Pereira, O., Fernández-Lucio, P., Fernández-Valdivielso, A.: Prediction of cutting forces including tool wear in high-feed turning of Nimonic® C-263 superalloy: a geometric distortion-based model. Measurement **211**, 112580 (2023). https://doi.org/10.1016/j.measurement.2023.112580
45. Özdemir, M., Şahinoğlu, A., Rafighi, M., Yilmaz, V.: Analysis and optimisation of the cutting parameters based on machinability factors in turning AISI 4140 steel. Can. Metall. Q. **61**(4), 407–417 (2022). https://doi.org/10.1080/00084433.2022.2058154
46. de Souza, L.G.P., Gomes, J.E.M., Arruda, É.M., Silva, G., de Paiva, A.P., Ferreira, J.R.: Evaluation of trade-off between cutting time and surface roughness robustness regarding tool wear in hard turning finishing. Int. J. Adv. Manuf. Technol. **123**(9), 3047–3078 (2022). https://doi.org/10.1007/s00170-022-10354-5
47. Prasad, G., Vijay, G.S., Kamath, R.C., Hemmady, H.J.: Optimization of the tool wear and surface roughness in the high-speed dry turning of Inconel 800. Cogent Eng. **11**(1), 2308993 (2024). https://doi.org/10.1080/23311916.2024.2308993
48. Ngoc, T.B., Duc, T.M., Tuan, N.M., Long, T.T.: Influence of Al2O3/MoS2 hybrid nanofluid MQL on surface roughness, cutting force, tool wear and tool life in hard turning. Forces Mech. **16**, 100285 (2024). https://doi.org/10.1016/j.finmec.2024.100285
49. Fountas, N.A., Manolakos, D.E., Vaxevanidis, N.M.: Machinability assessment and multi-objective optimization of Graphene Nanoplatelets-reinforced aluminum matrix composite in dry CNC turning. Metals **15**(6), 584 (2025). https://doi.org/10.3390/met15060584
50. Laghari, R.A., Sarhan, A.A.D.: Parametric modeling and optimization for machinability performance enhancement of difficult-to-cut SiCp/Al (50%) MMCs using ANFIS and MRA. Int. J. Interact. Des. Manuf. (IJIDeM) (2025). https://doi.org/10.1007/s12008-025-02282-x
51. Butola, R., Sharma, V., Kanwar, S., Tyagi, L., Singari, R.M., Tyagi, M.: Optimizing the machining variables in CNC turning of aluminum-based hybrid metal matrix composites. SN Appl. Sci. **2**(8), 1356 (2020). https://doi.org/10.1007/s42452-020-3155-8
52. Tiwari, S., Amarnath, M.: Improving the machining performance with bio-degradable coconut oil-assisted MQL turning of AISI-1040 steel: a sustainable machining approach. Biomass Convers. Biorefin. **14**(19), 24731–24751 (2024). https://doi.org/10.1007/s13399-023-04573-3
53. Bacha, M., Elbah, M., Laouici, H., Yallese, M.A., Sassi, H.: Enhancing the hard turning performance of AISI 02 steel with CuO nanocutting fluids. Int. J. Adv. Manuf. Technol. (2025). https://doi.org/10.1007/s00170-025-15063-3
54. Nguyen, V.C., Tien, D.H., Pham, V.H., Nguyen, T.V., Nguyen, T.D.: Toward sustainable machining of hardened SKD11: machine learning-based evaluation and optimization of surface roughness, tool wear, and CO_2 emissions. Results Eng. (2025). https://doi.org/10.1016/j.rineng.2025.105249
55. Derani, M.N., Ratnam, M.M.: The use of tool flank wear and average roughness in assessing effectiveness of vegetable oils as cutting fluids during turning—a critical review. Int. J. Adv. Manuf. Technol. **112**, 1841–1871 (2021). https://doi.org/10.1007/s00170-020-06490-5
56. Laghari, R.A., Jamil, M., Laghari, A.A., Khan, A.M., Akhtar, S.S., Mekid, S.: A critical review on tool wear mechanism and surface integrity aspects of SiCp/Al MMCs during turning: prospects and challenges. Int. J. Adv. Manuf. Technol. **126**(7), 2825–2862 (2023). https://doi.org/10.1007/s00170-023-11178-7
57. Pereira Guimaraes, B.M., da Silva Fernandes, C.M., de Amaral Figueiredo, D., da Correia Pereira Silva, F.S., Macedo Miranda, M.G.: Cutting temperature measurement and prediction in machining processes: comprehensive review and future perspectives. Int. J. Adv. Manuf. Technol. **120**(5), 2849–2878 (2022). https://doi.org/10.1007/s00170-022-08957-z
58. Reffas, O., Boumediri, H., Karmi, Y., Kahaleras, M.S., Bousba, I., Aissa, L.: Statistical analysis and predictive modeling of cutting parameters in EN-GJL-250 cast iron turning: application of machine learning and MOALO optimization. Int. J. Adv. Manuf. Technol. (2025). https://doi.org/10.1007/s00170-025-15098-6
59. Liu, H., Meurer, M., Bergs, T.: Experimental and finite element analysis of adapted cutting fluid supply on tool temperature and wear progression in Inconel 718 turning. J. Manuf. Process. **137**, 166–180 (2025). https://doi.org/10.1016/j.jmapro.2025.01.061
60. Herrera Fernández, M., Martín-Béjar, S., Sevilla Hurtado, L., Trujillo Vilches, F.J.: Optimizing cutting parameters for enhanced control of temperature, cutting forces, and energy consumption in dry turning of Ti6Al4V alloy. Materials **18**(5), 942 (2025). https://doi.org/10.3390/ma18050942
61. Yağmur, S.: The effects of cooling applications on tool life, surface quality, cutting forces, and cutting zone temperature in turning of Ni-based Inconel 625. Int. J. Adv. Manuf. Technol. **116**(3), 821–833 (2021). https://doi.org/10.1007/s00170-021-07489-2
62. Aboloje, A.E., Sada, S.O.O., Ekpu, M., Eyenubo, J.: Evaluation of the optimal cutting performance of high-speed steel and tungsten carbide cutting tools in the machining of AISI 304 steel. Int. J. Adv. Manuf. Technol. **130**(7), 3609–3617 (2024). https://doi.org/10.1007/s00170-023-12909-6
63. Van-Canh, N., Anh-Thang, N., Ngoc-Linh, P., Thuy-Duong, N.: Multi-objective optimization of SUS430C steel turning process using hybrid machine learning and evolutionary algorithm approach. Results Eng. (2025). https://doi.org/10.1016/j.rineng.2025.104233
64. Oussama, B., Yapan, Y.F., Uysal, A., Abdelhakim, C., Mourad, N.: Assessment of turning AISI 316L stainless steel under MWCNT-reinforced nanofluid-assisted MQL and optimization of process parameters by NSGA-II and TOPSIS. Int. J. Adv. Manuf. Technol. **127**(7), 3855–3868 (2023). https://doi.org/10.1007/s00170-023-11747-w
65. Saatçi, E., Yapan, Y.F., Uysal, M.U., Uysal, A.: Orthogonal turning of AISI 310S austenitic stainless steel under hybrid nanofluid-assisted MQL and a sustainability optimization using NSGA-II and TOPSIS. Sustain. Mater. Technol. **36**, e00628 (2023). https://doi.org/10.1016/j.susmat.2023.e00628
66. Khelfaoui, F., Yallese, M.A., Boucherit, S., Ouelaa, N., Belhadi, S., Ben Salem, S.: Assessment of performance parameters in intermittent turning and multi-response optimization of machining conditions using DF, MOORA, VIKOR, and coupled NSGAII-VIKOR methods. Int. J. Adv. Manuf. Technol. **130**(11), 5665–5691 (2024). https://doi.org/10.1007/s00170-024-12979-0
67. Sen, B., Kumar, R., Kanabar, B., Kedia, A., Kumar, A.V., Bhowmik, A.: Comparative analysis of NSGA-II and TLBO for optimizing machining parameters of Inconel 690: a sustainable manufacturing paradigm. J. Mater. Eng. Perform. (2024). https://doi.org/10.1007/s11665-024-10539-x
68. Bennett, K.S., DePaiva, J.M., Lazar, E., Veldhuis, S.C.: Leveraging metaheuristic algorithms with improved hybrid prediction model framework for enhancing surface roughness optimization in CNC turning AISI 316. Int. J. Adv. Manuf. Technol. **135**(5), 1955–1983 (2024). https://doi.org/10.1007/s00170-024-14654-w
69. Saha, S., Zaman, P.B., Tusar, M.I.H., Dhar, N.R.: Multi-objective genetic algorithm (MOGA) based optimization of high-pressure coolant assisted hard turning of 42CrMo4 steel. Int. J. Interact. Des. Manuf. (IJIDeM) **16**(3), 1253–1272 (2022). https://doi.org/10.1007/s12008-022-00848-7
70. Kazeem, R.A., Fadare, D.A., Ikumapayi, O.M., Adediran, A.A., Aliyu, S.J., Akinlabi, S.A., Jen, T.C., Akinlabi, E.T.: Advances

in the application of vegetable-oil-based cutting fluids to sustainable machining operations—a review. Lubricants **10**(4), 69 (2022). https://doi.org/10.3390/lubricants10040069
71. Ponnusamy, P., Tamilperuvalathan, S.: Performance evaluation and hybrid deep recurrent neural network-based prediction of SS304 turning characteristics using nanoparticles added water emulsified MQL. Biomass Convers. Biorefin. **13**(8), 7349–7373 (2023)
72. Gupta, M.K., Mia, M., Pruncu, C.I., Khan, A.M., Rahman, M.A., Jamil, M., Sharma, V.S.: Modeling and performance evaluation of Al2O3, MoS2 and graphite nanoparticle-assisted MQL in turning titanium alloy: an intelligent approach. J. Braz. Soc. Mech. Sci. Eng. **42**(4), 207 (2020). https://doi.org/10.1007/s40430-020-2256-z
73. Haghnazari, S., Abedini, V.: Effects of hybrid Al2O3–CuO nanofluids on surface roughness and machining forces during turning AISI 4340. SN Appl. Sci. **3**(2), 203 (2021)
74. Dhanalakshmi, S., Rameshbabu, T.: Comparative study of parametric influence on wet and dry machining of LM 25 aluminium alloy. Mater. Today Proc. **39**, 48–53 (2021). https://doi.org/10.1016/j.matpr.2020.06.101
75. Kumar, T.S., Shalini, S., Kumar, K.K., Thavamani, R., Subramanian, R.: Bagasse ash reinforced A356 alloy composite: synthesis and characterization. Mater. Today Proc. **5**(2), 7123–7130 (2018). https://doi.org/10.1016/j.matpr.2017.11.377
76. Palanivendhan, M., Chandaradass, J., Philip, J.: Fabrication and mechanical properties of aluminium alloy/bagasse ash composite by stir casting method. Mater. Today Proc. **45**, 6547–6552 (2021). https://doi.org/10.1016/j.matpr.2020.11.458
77. Shankar, S., Balaji, A., Kawin, N.: Investigations on mechanical and tribological properties of Al-Si10-Mg alloy/sugarcane bagasse ash particulate composites. Particu. Sci. Technol. **36**(6), 762–770 (2018). https://doi.org/10.1080/02726351.2017.1301609
78. Demisie, L.F., Getnet, E., Taddese, G.A., Rengiah, R.G., Takele, T.N., Ayalew, Y.G., Berihun, E.A.: Experimental analysis on the mechanical properties of Al6061 based hybrid composite reinforced with silicon carbide, bagasse fly ash and aloe vera ash. Discover Appl. Sci. **6**(9), 491 (2024). https://doi.org/10.1007/s42452-024-06192-7